Available online at www.sciencedirect.com

ScienceDirect

Geochimica et Cosmochimica Acta 250 (2019) 191–208

Geochimica et Cosmochimica Acta

www.elsevier.com/locate/gca

Multi-colony coral skeletal Ba/Ca from Singapore's turbid urban reefs: Relationship with contemporaneous in-situ seawater parameters

J.T.I. Tanzil [a,b,c,*], N.F. Goodkin [a,b], T.M. Sin [c], M.L. Chen [a,b], G.N. Fabbro [b], E.A. Boyle [d,e], A.C. Lee [c], K.B. Toh [f]

[a] *Asian School of the Environment, Nanyang Technological University, Singapore*
[b] *Earth Observatory of Singapore, Nanyang Technological University, Singapore*
[c] *Tropical Marine Science Institute, National University of Singapore, Singapore*
[d] *Singapore-MIT Alliance in Research and Technology, Singapore*
[e] *Department of Earth, Atmospheric and Planetary Science, Massachusetts Institute of Technology, Boston, USA*
[f] *School of Natural Resources and Environment, University of Florida, Florida, USA*

Received 17 April 2018; accepted in revised form 18 January 2019; available online 1 February 2019

Abstract

The ratio of barium to calcium in coral skeletons (Ba/Ca_{coral}) is broadly used as a proxy for tracking terrestrial/river runoff. There are, however, inconsistencies in Ba/Ca_{coral} records that have prompted caution in its reliability as an environmental proxy. Direct comparisons between *in-situ* seawater measurements and coral Ba/Ca are therefore needed to ensure accurate proxy calibration and interpretation. The current study represents the first to test Ba/Ca_{coral} against years-long monthly-resolution contemporaneous measurements of several *in-situ* seawater parameters i.e. dissolved seawater barium (Ba_{SW}), temperature, salinity, suspended sediments, sedimentation rate and photosynthetically active radiation. We analysed the Ba/Ca_{coral} of six *Porites lutea* corals sampled from two turbid reefs in Singapore, and explored relationships with *in-situ* seawater parameters over the period 2008–2015. Our study found poor agreement in Ba/Ca_{coral} from replicate corals sampled from the same reef, and only one of the six colonies analysed showed significant but weak Ba/Ca_{coral}–Ba_{SW} and Ba/Ca_{coral}–Ba/Ca_{SW} relationships. There was also no clear relationship between Ba/Ca_{coral} and skeletal luminescence G/B (a coral proxy strongly linked with salinity and river runoff). This implies that (1) the incorporation of terrestrially derived humic-like substances into the coral is independent of Ba, and (2) it is likely factors other than freshwater discharge/flood events are driving the poor reproducibility of Ba/Ca_{coral} and disconnect with Ba_{SW} at our study sites. We found a positive relationship between Ba/Ca_{coral} and organic suspended solids for 4 of the 6 colonies analysed that suggests biological mechanisms such as feeding could be driving skeletal Ba incorporation. A negative relationship between Ba/Ca_{coral} and total sedimentation rate was also found, suggesting that within reef sediment fluxes may be influencing spatio-temporal variability of the Ba-supply. Ba incorporation into coral skeleton, especially in dynamic, turbid settings such as those found in Singapore, is likely more complex than previously thought. Our results highlight the possibility of high heterogeneity in coral responses to environmental conditions, and the need for careful selection of colonies and a site-specific, replicated approach when attempting to apply Ba/Ca_{coral} as a trace element proxy.

Keywords: Barium; Calcium; *Porites lutea*; Luminescence; Singapore; Salinity; Sediments; Water quality

* Corresponding author at: Asian School of the Environment, Nanyang Technological University, N2-01c-36, 50 Nanyang Avenue, Singapore 639798, Singapore.
E-mail address: jani.tanzil@nus.edu.sg (J.T.I. Tanzil).

https://doi.org/10.1016/j.gca.2019.01.034
0016-7037/

1. INTRODUCTION

There is rising concern that the rates of human-induced declines in coastal water quality worldwide could exceed the adaptive capacity of important yet sensitive marine ecosystems such as coral reefs (Nicholls et al., 2007). Therefore, great impetus exists to understand the impacts of environmental change on the health and resilience of key ecosystem engineers (e.g. reef-building corals) and the conditions needed to ensure their continued survival. Establishing the impacts of historical stress and disturbances, and any subsequent ecosystem recovery, are key to anticipating the effects of future environmental changes. The inclusions of trace elements into the skeletons of long-lived, annually banded, reef-building corals provide the unique opportunity to chronologically reconstruct past environmental conditions under which their growth occurred (Tudhope et al., 1996; Goodkin et al., 2005; Lough, 2010). Skeletal proxies circumvent the spatio-temporal limitations of instrumental records and provide insight into long-term anthropogenic and climatic impacts on water quality and, in turn, ecosystems. For example, the ratio of strontium to calcium (Sr/Ca) in coral skeleton has been shown to respond predictably to changes in sea temperature, and is used extensively as a proxy-based paleo-thermometer (Shen et al., 1996; Alibert and McCulloch, 1997; Marshall and McCulloch, 2002; Goodkin et al., 2005; Bolton et al., 2014).

An elemental tracer broadly used as a proxy for changes to near-shore water quality driven by terrestrial/river runoff, coastal activities and proximal land use changes is the ratio of barium to calcium (Ba/Ca) in coral skeleton (Alibert et al., 2003; Sinclair and McCulloch, 2004; Fleitmann et al., 2007; Carriquiry and Horta-Puga, 2010; Maina et al., 2012; Moyer et al., 2012; Prouty et al., 2014; Brenner et al., 2017; Lewis et al., 2018). Although the marine Ba biogeochemical cycle is not fully understood (Dymond et al., 1992; Paytan and Kastner, 1996; Dickens et al., 2003), the major external source of Ba in seawater in coastal environments is terrestrial/riverine input (Goldstein and Jacobsen, 1988). Transport of freshwater plumes (e.g. river discharge) towards the ocean brings barium-rich terrestrial-sourced particulates (e.g. clay minerals), which desorb Ba upon contact with more saline waters and contribute to the total dissolved Ba in seawater (Ba_{SW}) (Hanor and Chan, 1977; Coffey et al., 1997). In coastal areas affected by upwelling, Ba from enriched deeper waters can also constitute a significant source of Ba to surface waters in addition to riverine inputs (Lea et al., 1989; Montaggioni et al., 2006).

Corals exposed to Ba enrichment incorporate Ba into their aragonite calcium carbonate ($CaCO_3$) skeletons as they grow via what appears to be relatively simple ionic substitution (i.e. Ba^{2+} substitutes for Ca^{2+} in proportion to the aqueous Ba/Ca). Several studies have shown that the partition coefficient of Ba (D_{Ba})—the ratio of Ba/Ca in the calcium carbonate coral skeleton (Ba/Ca_{coral}) to Ba/Ca in seawater (Ba/Ca_{SW})—for different species living in varied environments is close to 1 (~1–1.4) (Lea et al., 1989; Lea and Spero, 1992; Alibert et al., 2003; Dietzel et al., 2004; LaVigne et al., 2011; Walther et al., 2013; LaVigne et al., 2016). This implies a lack of influence by vital effects (biological factors) and that Ba/Ca in coral skeletons can potentially be used to systematically reflect ambient seawater Ba.

In coastal regions, flood events present the most robust relationship to coral Ba/Ca as they carry fresh sediment-laden water from rivers (Alibert et al., 2003; McCulloch et al., 2003; Sinclair and McCulloch, 2004). Long-term trends and peaks in coral Ba/Ca have also been shown to closely match trends and peaks in skeletal luminescence (Alibert et al., 2003; Sinclair and McCulloch, 2004; Grove et al., 2010; Grove et al., 2012) another coral derived record that correlates well with terrestrial riverine and freshwater inputs (Boto and Isdale, 1985; Susic et al., 1991; Zicheng et al., 2002; Grove et al., 2010; Grove et al., 2012; Llewellyn et al., 2012, Tanzil et al., 2016). The principle cause of the skeletal luminescence proposed in this case is the incorporation in the coral skeleton of fluorophores, specifically humics/humic-like substances, leached from the terrestrial environment (Boto and Isdale, 1985; Susic et al., 1991; Zicheng et al., 2002; Grove et al., 2010; Grove et al., 2012; Llewellyn et al., 2012; Tanzil et al., 2016). Such correlations between coral Ba/Ca and luminescence further support coral Ba/Ca as a proxy for terrestrial/riverine inputs in coastal environments.

Despite Ba/Ca being widely used as a tracer for terrestrial discharge, there is, however, still uncertainty surrounding its reliability. Several studies comprehensively reviewed by Saha et al. (2016) reported anomalous coral Ba/Ca records that do not correspond with estimated changes in seawater Ba based on known aspects of Ba biogeochemical cycling, and prompt caution in the use and interpretation of Ba/Ca as a coral proxy. For example, Sinclair (2005) found Ba/Ca behaviour differed in *Porites* corals taken from Great Barrier Reef (GBR) reefs <30 km apart despite both being thought to be predominantly influenced by discharge from the Burdekin river. Poor replication of Ba/Ca ratios recorded by duplicate coral colonies from the same reef has also been reported (Lewis et al., 2018). In such cases, explanations provided centre around the possibilities that particular environments are affected by non-riverine barium and/or exert a control on the corals' physiology (i.e. vital effects). Direct comparisons between *in-situ* seawater measurements and coral Ba/Ca are therefore crucial in order to ensure valid proxy calibrations and reconstructions of any environment.

In this study, we explore the skeletal Ba/Ca in six *Porites lutea* corals from two highly-sedimented turbid near-shore reefs in Singapore, with the specific aim to assess the potential of using coral Ba/Ca as proxy for past reef water quality in Singapore. The prevalence of massive *Porites lutea* colonies around Singapore (Leng and Lim, 1990; Goh and Chou, 1993; Guest et al., 2016), along with the availability of a suite of years-long (2008–2015) monthly water quality data (taken as part of a long-term environmental monitoring programme), provides a unique opportunity to establish multi-colony calibrations with contemporaneous *in-situ* seawater measurements.

2. MATERIALS AND METHODS

2.1. Study location and climate setting

With a land area of ~720 km^2 and a population of ~5.6 million, Singapore is amongst the most densely populated countries in the world (Singstat, 2016). The inevitable consequences of Singapore's acute land scarcity and high population density are the results of conversion of undisturbed natural areas for housing, infrastructure and industry, including large-scale sea reclamation projects that began in the 1960s (Lu et al., 2005; Koh and Lin, 2006). Once covering an area of >100 km^2, Singapore's remaining ~13.25 km^2 of coral reefs now largely occur as fringing and patch reefs around the southern islands and co-exist alongside industries, busy ports and shipping channels (Burke et al., 2002; Tun, 2012). These reefs are therefore subject to high levels of local natural and anthropogenic disturbances that result in a highly turbid reef environment. Sedimentation levels on Singapore's reefs increased from ~3–6 mg cm^{-2} day^{-1} in 1979 up to ~5–45 mg cm^{-2} day^{-1} in more recent years (Low and Chou, 1994; Dikou and van Woesik, 2006), and underwater visibility reduced from ~10 m in the 1960s to 2 m or less today (Tun et al., 1994; Dikou and van Woesik, 2006; Tun, 2012).

Singapore lies at the southern tip of the Thai-Malay Peninsula (Fig. 1) on the inner continental Sunda shelf of the South China Sea in shallow waters less than ~30 m (Bird et al., 2006). The Titiwangsa mountain range runs through the middle of the Peninsula rising to ~2100 m with short, swift-flowing rivers running east and west perpendicular to the mountain range (Fig. 1). Foothills of the Titiwangsa mountain range extend to the southern part of the Peninsula, where gentler slopes and advanced erosion form relatively slower-moving rivers with ill-defined channels, and marshes and swamps that extend far inland from the coasts (Hutchinson and Tan, 2009). High year-round precipitation ensures perennial river flow in this region, with torrential (and often localised) rainfall patterns during the wet season causing rapid fluctuations in discharge that result in considerable run-off and substantial loads of riverine material being transported to coastal waters.

The climate in Singapore can be divided into the wet (average rainfall ~300 mm month^{-1}) northeast (NE) monsoon period (November–March), drier (average rainfall ~150 mm month^{-1}) southwest (SW) monsoon (May–September) and the inter-monsoon (IM) periods (April and October) (Tanzil et al., 2016). Winds in Singapore are relatively light (maximum wind speeds <3 m s^{-1}) throughout the year and seas are calm, due to both latitude and the sheltering effects from Sumatra to the west and the Thai-Malay Peninsula to the north. Regional monsoonal winds do, however, drive net seawater transport across Singapore – wind-driven circulation forces more saline, clearer waters from the South China Sea to the Singapore Straits during the NE monsoon, while the SW monsoon allows intrusion of more turbid, lower salinity waters from the Malacca Straits (Rizal et al., 2012; Sin et al., 2016). This alternating monsoon current effectively drives the decoupling of local rainfall and salinity in the Singapore Straits i.e. counterintuitive salinity minima observed during the drier SW monsoon period and higher salinities during the wetter NE monsoon (see Tanzil et al., 2016).

2.2. Coral and seawater sample collection

Cores (30–70 cm) from six live massive *Porites lutea* colonies were sampled between May 2014 and April 2016 from two sites – Pulau Kusu (KU: 1.22549°N, 103.74054°E) and Pulau Hantu (HT: 1.22729°N, 103.74664°E) (Fig. 1) located within the Singapore Straits (~5 km from main island of Singapore). The three replicate colonies from

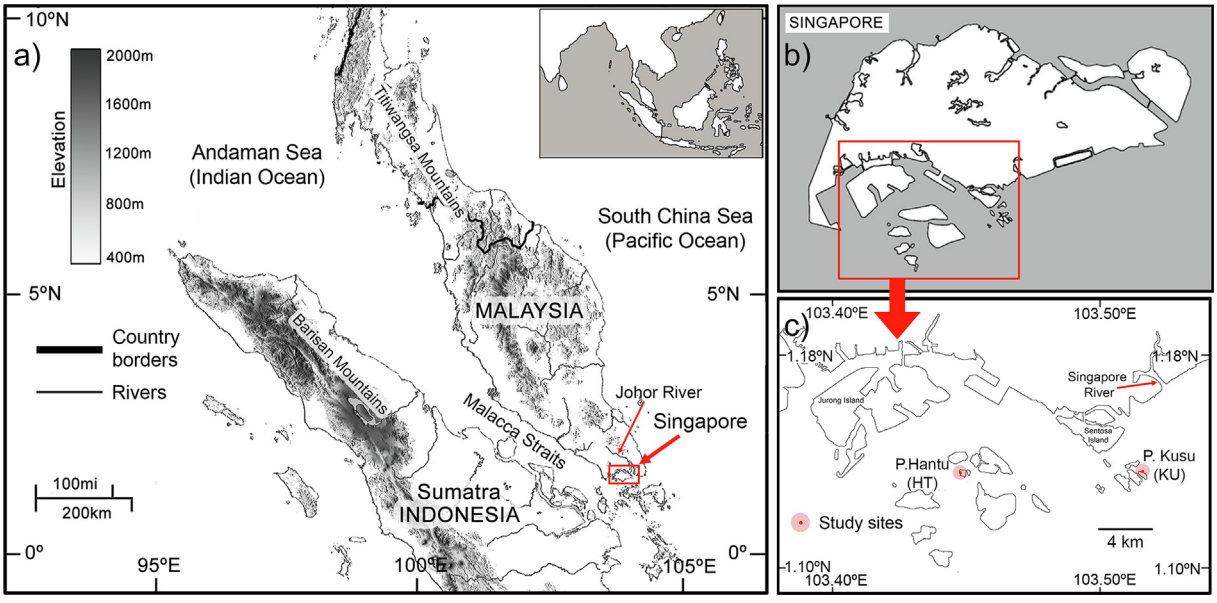

Fig. 1. Map of Southeast Asia (a), Singapore (b) and Pulau Kusu (KU) and Hantu (HT) (c). (Pulau means island in Malay.)

each of the study sites were within ~10 m of one another. All samples were taken from the main growth axis of the colony using a pneumatic drill fitted with a 5 cm diameter, 50 cm long diamond bit core barrel from ~2–3 m below mid-tide height (tidal range: ~3 m) from colonies ~0.5–2 m in diameter. Slices (~7 mm thick) were obtained from these cores for skeletal luminescence and Ba/Ca analyses.

Seawater parameters at the two study sites were sampled at monthly frequency over variable periods between September 2008 and December 2015 (Table 1). These include salinity (psu), temperature (°C), total suspended solids (TSS; mg l^{-1}), total sedimentation rate (TSD; mg cm^{-2} day^{-1}), photosynthetically active radiation (PAR) and barium concentration (Ba_{SW}; nmol kg^{-1}). Salinity and temperature were measured monthly from September 2008–December 2015 using a YSI 6600 multi-parameter sonde at 1 m below sea surface. TSS and TSD were measured from March 2010–December 2015. TSS was measured from discrete water samples (1 litre) obtained via SCUBA approximately 50–70 cm above the reef bed where sampled coral colonies resided. TSD, representing the gross downward flux of particulate matter, was quantified using cylindrical sediment traps 30 cm in length, with an internal diameter of 5 cm. These sediment traps were deployed monthly at ~3 m depth at mid-tide and approximately 30 cm from the reef bed. Samples for TSS and TSD were vacuum filtered in the laboratory on pre-weighed glass fibre filter paper (Millepore AP400, pore size 0.7 μm) and dried at 105 °C for 24 hours. TSS and TSD were also analysed for their organic (OSS/OSD) and inorganic constituents (ISS/ISD), by combusting samples at 550 °C to remove organic matter and measuring the difference in dry weights pre- and post- combustion. Average photosynthetically active radiation (PAR; μmol m^{-2} day^{-1}) (monthly average for 1000–1400 hrs) was measured using Odyssey light loggers (model number Z412, calibrated against LiCOR LI-192 PAR sensor) deployed *in-situ* at 3 m depth at mid-tide with data collection set at half hourly intervals. PAR loggers were retrieved for download and calibration at monthly intervals. PAR data were examined carefully for indications of signal decay, signal-to-noise ratio and changes in standard deviation. Typically, *in-situ* readings were reliable for ~5 days, after which biofilm formation and settlement of suspended material onto sensor surfaces impacted data reliability. Discrete seawater sub-surface seawater samples for Ba_{SW} were obtained monthly for the period July 2011–December 2013. Samples were filtered and acidified following trace metal clean procedures (Chen et al., 2015).

2.3. Coral and seawater sample analyses

All coral slices were cleaned (mild oxidative treatment) for 48 hours in a 1:4 mix of commercially available

Table 1
Average ± 1 SD and data period for salinity, temperature, total suspended solids (TSS; mg l^{-1}), inorganic suspended solids (ISS; mg l^{-1}), organic suspended solids (OSS; mg l^{-1}), total sedimentation rate (TSD; mg cm^{-2} day^{-1}), inorganic sedimentation rate (ISD; mg cm^{-2} day^{-1}), organic sedimentation rate (OSD; mg cm^{-2} day^{-1}), photosynthetically active radiation (PAR; μmol m^{-2} day^{-1}) and dissolved barium seawater (Ba_{SW}; nmol kg^{-1}) at each study site (Pulau Hantu – HT; Pulau Kusu – KU), and average annual linear extension rates (LE) and Ba/Ca ratios for each of the replicate *Porites lutea* coral (HT-G, HT-H, HT-I and KU-F, KU-K, KU-L).

Site/Sample	Parameter	Average ± SD	Data period
P. Hantu	Salinity	31.071 ± 0.957	September 2008–December 2015
(HT)	Temperature	29.368 ± 0.973	September 2008–December 2015
	TSS	21.964 ± 15.282	March 2010–December 2015
	– ISS	16.954 ± 11.961	March 2010–December 2015
	– OSS	5.010 ± 4.096	March 2010–December 2015
	TSD	8.000 ± 5.407	March 2010–December 2015
	– ISD	6.028 ± 4.613	September 2011–December 2015
	– OSD	0.448 ± 0.350	September 2011–December 2015
	PAR	261.367 ± 106.384	March 2010–December 2015
	Ba_{SW}	52.359 ± 5.340	July 2011–December 2013
HT-G	Ba/Ca	4.356 ± 1.287	December 2008–December 2012
HT-H	Ba/Ca	6.218 ± 1.557	April 2011–November 2015
HT-I	Ba/Ca	5.003 ± 2.250	April 2011–September 2015
P. Kusu	Salinity	31.199 ± 0.830	September 2008–December 2015
(KU)	Temperature	29.499 ± 1.073	September 2008–December 2015
	TSS	22.833 ± 16.110	March 2010–December 2015
	– ISS	17.3616 ± 11.747	March 2010–December 2015
	– OSS	5.471 ± 4.968	March 2010–December 2015
	TSD	15.645 ± 8.262	March 2010–December 2015
	– ISD	12.892 ± 7.205	September 2011–December 2015
	– OSD	1.077 ± 0.545	September 2011–December 2015
	PAR	295.542 ± 131.809	March 2010–December 2015
	Ba_{SW}	52.337 ± 5.107	July 2011–December 2013
KU-F	Ba/Ca	6.052 ± 2.583	December 2008–March 2013
KU-K	Ba/Ca	4.728 ± 2.828	December 2008–May 2015
KU-L	Ba/Ca	5.840 ± 1.516	December 2008–November 2015

household bleach solution (NaOCl, 3–7 % reactive chlorine) and water to remove surficial organic contaminants (Nagtegaal et al., 2012) and sonicated in deionised water for a total of 30 minutes (water changed every 10 min). The slices were then photographed under ultraviolet (UV) light (365 nm wavelength; 450 nm light cut-off camera filter) using spectral line scanning (SLS) and the ratio of the green to blue spectral components (G/B) was used as a measure of luminescence intensity (Grove et al., 2010; Tanzil et al., 2016). Luminescence G/B for each coral sample was obtained along the main growth axis for a ~0.2 cm wide track and at a resolution of 72 pixels cm^{-1} (i.e. at every ~ 0.014 cm).

Laser ablation inductively coupled mass spectrometry (LA-ICP-MS) was then used to measure the skeletal barium to calcium ratios (Ba/Ca) in all coral samples. The coral slices were sectioned into ~15 cm lengths and mounted on a custom stage alongside reference standards, and analysed using a Thermo Scientific iCAP Quadrupole ICP-MS coupled to a Photon Machines Analyte G2 193 nm excimer laser. Laser ablation transects were set along the major growth axis of the coral slice, overlapping the track measured for luminescence G/B. The laser spot size was 150 × 150 μm with a scan speed of 20 μm s^{-1} and a repetition rate of 10 Hz, yielding a sampling resolution of 2 μm. Before analysis, each sample was pre-ablated to expose fresh aragonite. At least 30 seconds of background was measured before and after each analysis and background signal obtained was subtracted from the raw signal recorded during analysis of the standards and samples using Iolite (The Iolite Team, 2017). Ba/Ca concentration ratios were calculated using the signal for ^{138}Ba and ^{43}Ca, calibrated using the NIST 610 glass standard, and were smoothed using a 100-point moving average (equivalent to 0.2 mm of coral). Ba/Ca measurements overlapping areas of coral tissue (i.e. track length overlapping measured tissue thickness) were discarded. Overall reproducibility for Ba/Ca, based on NIST 612 glass standard measurements run after every NIST 610 measurement, was 3.7 % SD. To further validate the accuracy of the LA-ICP-MS results, comparisons were made between laser and solution ICP-MS analyses of drilled/milled samples obtained at every 0.5 mm adjacent to the laser track for one coral slab (KU-F) (see Supporting Information). Results from both laser and solution methods returned highly comparable ($r^2 = 0.79$) average Ba/Ca values and temporal patterns (Fig. S1), although peaks in Ba/Ca obtained from laser method were notably higher than those found from solution analysis – possibly as a result of the higher sampling resolution of the laser. To test whether the coral cleaning method used in the current study sufficiently removed any non-skeletal residues that could affect Ba/Ca signals, we compared the Ba/Ca of paired samples cleaned using NaOCl vs. a more rigorous oxidative cleaning method using HNO_3 and H_2O_2 (modified by Shen and Boyle, 1988). Other than samples obtained from the coral tissue layer, both methods yielded highly comparable Ba/Ca results (Fig. S2). Consequently, we concluded that the NaOCl cleaning was sufficient to exclude residual Ba/Ca signals from any non-skeletal matrix organic matter except from within the coral tissue layer. As such, any data from, and immediately beneath, the surface coral tissue layer were excluded.

Acidified filtered seawater samples were diluted by a factor of 50 and analysed for dissolved barium (Ba_{SW}) using a standard curve and standard spike method on a triple-quad ICP-MS (ICP-QQQ, Agilent 8800 at the Singapore-MIT Alliance in Research and Technology). Samples were prepared volumetrically by diluting 50 μl of sample in 2425 μl of 0.1 M ultrapure HNO_3 and spiked with 25 μl of 1 μg l^{-1} indium as an internal standard. Indium-spiked multi-element standard (Ba, Sr, Mg) was gravimetrically prepared in 0.1 M ultrapure HNO_3 to establish a five-point standard calibration curve. All plastic ware used were trace metal cleaned following procedures in Chen et al. (2015). The blank, spiked procedural blank and spiked standard curve were analyzed after every five samples. The Ba concentrations in the samples were then calculated by comparing the Ba/In ratio in the sample vs. in the series of standards. The average standard deviation for this method was 1.18 nmol kg^{-1} based on duplicate samples. Ba/Ca_{SW} was then calculated based on salinity measurements and Ca as 1.2 % of salts in seawater.

2.4. Coral age model

Coral chronologies were based on the seasonal cycles of skeletal luminescence previously validated at these study sites using alizarin staining over a two-year period (for more details, see Tanzil et al., 2016). Briefly, coral slices were photographed under ultraviolet (UV) light (365 nm wavelength; 450 nm light cut-off camera filter) using spectral line scanning (SLS) and the ratio of the green to blue spectral components (G/B) was used as a measure of luminescence intensity (Grove et al., 2010; Tanzil et al., 2016). Luminescence G/B for each coral sample was obtained along the main growth axis for a ~0.2 cm wide track and at a resolution of 72 pixels cm^{-1} (i.e. at every ~0.014 cm). Monthly resolution datasets of luminescence were obtained using a method modified from Tanzil et al. (2016): all growth years identified were interpolated linearly using a luminescence intensity–salinity chronology alignment i.e. luminescence G/B maxima were matched to salinity minima and vice versa using AnalySeries 2.0 (Paillard et al., 1996). Luminescence G/B patterns were cyclical and highly reproducible among all the colonies sampled from the two study sites, and alignment resulted in a refined time scale of monthly resolution as defined by salinity with 12 equidistant data points (see Tanzil et al., 2016). The skeletal Ba/Ca (LA-ICP-MS) and luminescence intensity datasets for the six corals sampled spanned between 4–7 years from ~December 2008–November 2015 (Table 1).

2.5. Statistical analyses

Pearson's product-moment correlation coefficients (r) were used to determine the degree of linear correlation between (a) *in-situ* dissolved seawater barium (Ba_{SW}) and salinity, (b) Ba/Ca_{coral} relationship with Ba_{SW} and Ba/Ca_{SW}, and Ba/Ca_{coral} with luminescence G/B for each of

the replicate coral colonies. Initial relationships between Ba/Ca_{coral} and Ba_{SW}, salinity (Sal), sea temperature (Temp), total suspended solids (TSS), organic suspended solids (OSS), inorganic suspended solids (ISS), total sedimentation rate (TSD), organic TSD component (OSD), inorganic TSD component (ISD) and photosynthetically active radiation (PAR) for each of the replicate colonies were also explored using Pearson's correlations.

Subsequently, the Ba/Ca at each site and at the global (i.e. all sites) level was modelled using Linear Mixed Effects (LME) models (Wood, 2006) with a random intercept. The fixed predictors were *in-situ* seawater variables which include Sal, Temp, PAR, suspended solids (SS) (i.e. either TSS, OSS or ISS), and sedimentation rate (SD) (i.e. either TSD, OSD or ISD), while the random effect was "id" (individual colony). Due to the significant collinear relationship among the total, organic and inorganic components, only one of the components of SS and SD was used as a predictor to avoid unstable parameter estimates (Pinheiro and Bates, 2000). A continuous first-order autoregressive correlation structure was also incorporated into the model to account for temporal correlation between Ba/Ca data, or mismatch of data due to monthly spot measurements of seawater parameters. We heuristically tested all combinations of the predictors, including all possible two-way interaction terms while limiting the maximum predictors per model to five to reduce over-fitting. The best five models based on Akaike Information Criterion (AIC_C) were selected for each study site (i.e. HT and KU), and for all sites (All). The leave-one-out-cross-validation (LOOCV) method was then used to assess the predictive performance of the selected models (James et al., 2013). In brief, $(n-1)$ observations were used to estimate the parameters of a selected model and to predict the mean response of the left-out observations and its square error. This was repeated until all observations were left out once. Model fits were assessed using cross-validated root mean square error (RMSE), normalized root mean square error (NRMSE) and log-likelihood R^2. All statistical analyses were performed using the statistical program R (version 3.3.3) (R Core Team, 2014), using packages 'stats', 'nlme' (Pinheiro et al., 2017), 'glmulti' (Calcagno and Mazancourt, 2010) and MuMIn (Bartoń, 2013).

3. RESULTS

3.1. Seawater parameters

Mean monthly seawater temperature at Pulau Kusu and Pulau Hantu (Pulau means "island" in Malay and will henceforth be abbreviated to "P.") averaged ~29.4 °C with a small annual range of ~3 °C. Seasonally, temperatures peak ~ May/June with a smaller peak in October/November, and a minimum in January (Table 1; Fig. 2a). PAR on the reef at 3 m depth for both P. Kusu and P. Hantu were low, averaging only ~260 μmol m^{-2} day^{-1} (Table 1; Fig. 2b) and showed a bimodal annual pattern – maxima in March/April (>500 μmol m^{-2} day^{-1}) and October/November, and minima as low as ~50–80 μmol m^{-2} day^{-1} in June/July/August and December/January (Fig. 2b). Salinity at the study sites also followed a clear annual cycle with maxima ~ November and March (coinciding with the start and end of the NE monsoon), and a minimum ~ August (coinciding with the peak of the SW monsoon) (Fig. 2b). There is also a slight dip in salinity ~ December–February coinciding with Singapore's peak rainfall period (refer to Tanzil et al., 2016; Sin et al., 2016 for more details on drivers of Singapore's seasonal dynamics). Average monthly salinity was ~31 psu, with an annual range of ~3 psu (~28.5–32.5 psu) (Table 1, Fig. 2c). Monthly Ba_{SW} sampled over a 2.5-year period (July 2011–December 2013) averaged ~52 nmol kg^{-1} at the study sites (Table 1). Ba_{SW} averages and temporal patterns at the two sites were similar (Fig. 2d) and temporal variability in Ba_{SW} seems to generally track that of salinity (Fig. 2c/d).

Total suspended solids (TSS) and their organic (OSS) and inorganic (ISS) components at both study sites were very similar: TSS averaged 22–22.0 ± SD 15.2 mg l^{-1} at P. Hantu and 22.8 ± SD 16.1 mg l^{-1} at P. Kusu, organic material (OSS) constituted on average 22 ± SD 10 % and 23 ± SD 10 % of the TSS at P. Kusu and P. Hantu respectively, and inorganic suspended solids (ISS) averaged 77 ± SD 10 % of TSS at P. Hantu and 77 ± SD 13 % at P. Kusu (Table 1; Fig. 2e/g/i). TSS, OSS and ISS at the two study sites exhibited similar temporal patterns over the 6-year sampling period (2010–2015): while no clear intra-annual/seasonal patterns could be discerned, there was high inter-annual variability. Average annual TSS at the two sites ranged from ~12–38 mg l^{-1} in 2014 sampling period with lowest concentrations found in 2010 and highest in 2014 (Fig. 2e/g/i).

Total sedimentation rate (TSD) was, on average, higher at P. Kusu (15.6 ± SD 8.3 mg cm^{-2} day^{-1}) than at P. Hantu (~8.0 ± SD 5.4 mg cm^{-2} day^{-1}) (Table 1). The particulate matter obtained from sediment traps for TSD measurements comprised of mostly inorganics (ISD) (90 ± SD 12 % at P. Kusu; 92 ± SD 3 % at P. Hantu), with very low percentage of organics (OSD) (8 ± SD 3 % at P. Kusu; 8 ± SD 2 % at P. Hantu). Site-level temporal patterns in TSD, OSD and ISD showed similar general characteristics: no clear intra-annual/seasonal patterns and high inter-annual variability (Fig. 2f/h/i). Inter-annual variability was higher at P. Kusu than at P. Hantu – average annual TSD ranged from ~5–14 mg cm^{-2} day^{-1} at P. Hantu and ~8–24 mg cm^{-2} day^{-1} at P. Kusu. Highest average annual sedimentation rates were found in 2010 for both sites, and lowest in 2012 at P. Hantu and 2014 at P. Kusu.

3.2. Ba_{SW} relationship with salinity

Initial tests using Pearson's correlations found a significant (at $\alpha = 0.05$) relationship between dissolved barium in seawater (Ba_{SW}) and salinity (All: $P < 0.001$, $r = -0.50$). Site-level analyses revealed the Ba_{SW}-salinity relationship was significant for P. Hantu ($P < 0.001$, $r = -0.563$), but not at P. Kusu ($P = 0.14$, $r = -0.31$). However, closer inspection of the data indicated some non-linearity in the relationship between the two variables. Segmented regressions were then used to partition linear fits for the data according to salinity intervals as estimated using a

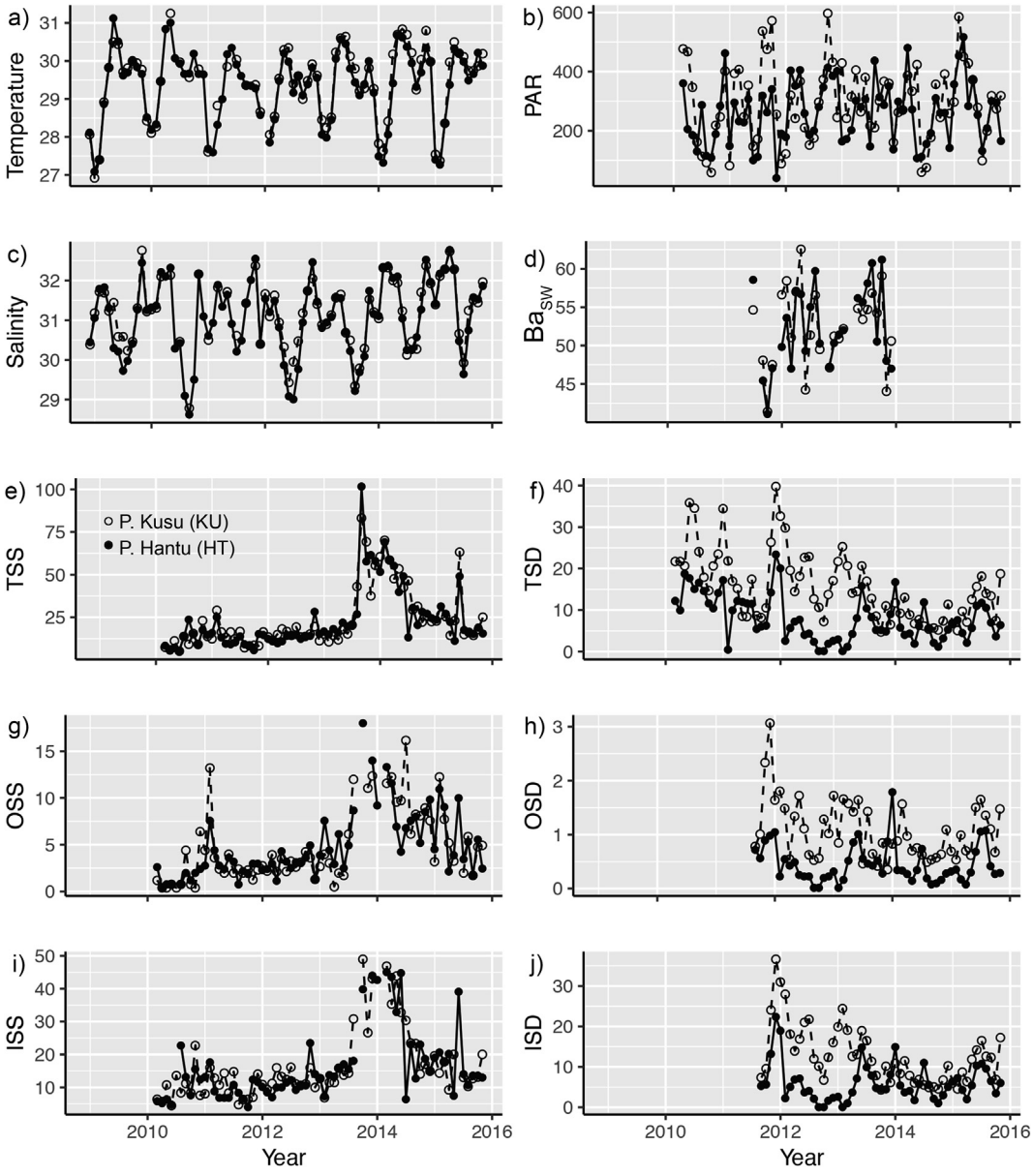

Fig. 2. Monthly *in-situ* (a) temperature (°C), (b) salinity (psu), (c) total suspended solids (TSS; mg l^{-1}), (d) organic suspended solids (OSS; mg l^{-1}), (e) inorganic suspended solids (ISS; mg l^{-1}), (f) sedimentation rate (mg cm^{-2} day^{-1}, (g) organic and (h) inorganic sedimentation rate (OSD, ISD; mg l^{-1}), (i) photosynthetically active radiation (PAR; µmol m^{-2} day^{-1}) and (j) barium seawater (Ba_{SW}; nmol/kg) for available periods within 2008–2016 for the two study sites. P. Kusu shown by open circles and dashed lines; P. Hantu by solid circles and solid lines.

maximum likelihood method (package 'segmented' in R) (Muggeo, 2008). The segment breakpoints were 30.10 ± 0.18 psu for P. Hantu, 30.32 ± 0.17 psu for P. Kusu, and 30.22 ± 0.14 psu when all sites were analysed together. Most of the data points below the salinity breakpoint values were identified as belonging to the months June, July and August (i.e. months during the peak of the SW monsoon) (Fig. 3). As such, separate ordinary least squares (OLS) regressions were then performed for data covering the months June–August and September–May. We found significant negative Ba_{SW}-salinity relationships for the September–May dataset (All: $P < 0.001$, $R^2 = 0.37$; KU: $P < 0.001$, $R^2 = 0.31$; HT: $P < 0.001$, $R^2 = 0.38$) (Fig. 3). In contrast, no relationship was found for the period June–August (All: $P = 0.57$; KU: $P = 0.34$; HT: $P = 0.51$) (Fig. 3). OLS regressions Ba_{SW}-salinity relationships (September–May) and their fits (R^2, and NRMSE, i.e. normalised residual mean square error) are summarised in Eqs. (1)–(3):

P. Hantu:

$$Ba_{SW}\ (\text{nmol kg}^{-1}) = 173.182(\pm 21.022) - 3.925(\pm 0.673) \times \text{Salinity (psu)}$$

$$(R^2 = 0.38, P < 0.001, n = 27, \text{NRMSE} = 17.7\%) \quad (1)$$

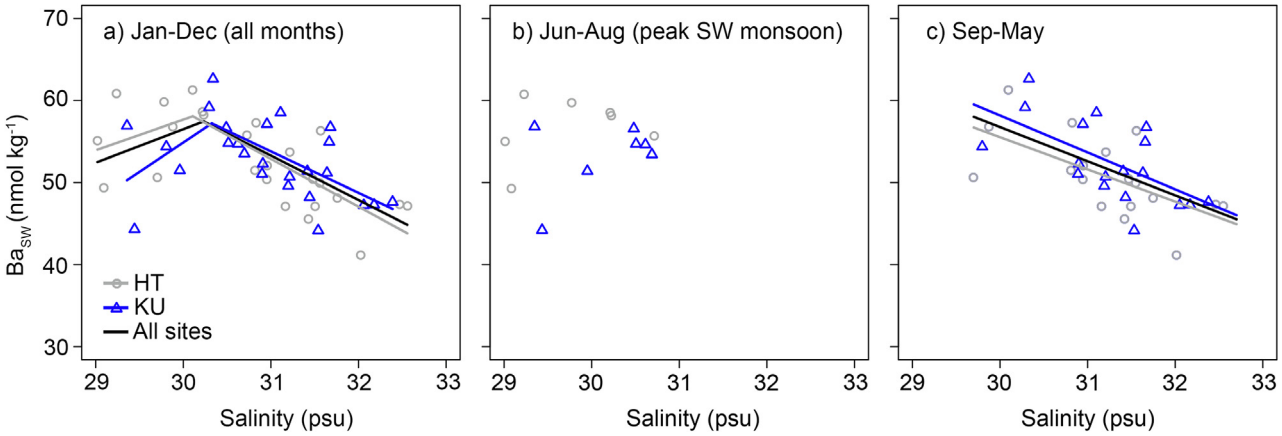

Fig. 3. Plots of dissolved barium seawater (Ba_{SW}; nmol kg^{-1}) vs. salinity (psu) at P. Kusu (KU; blue triangles) and P. Hantu (HT; gray circles) for the months of (a) January–December (i.e. all months), (b) June–August (i.e. peak southwest (SW) monsoon months), and (c) September–May, over the period Jul 2011–December 2013. Only significant regression lines (segmented and linear) are shown for P. Kusu (KU; blue line), P. Hantu (HT; gray line) and all sites (black line). (For interpretation of the references to colour in this figure legend, the reader is referred to the web version of this article.)

P. Kusu:

$$Ba_{SW}\ (\text{nmol kg}^{-1}) = 197.204(\pm 24.859) - 4.634(\pm 0.795) \times \text{Salinity (psu)}$$

$$(R^2 = 0.31, P < 0.001, n = 25, NRMSE = 18.4\%) \quad (2)$$

ALL:

$$Ba_{SW}\ (\text{nmol kg}^{-1}) = 182.213(\pm 16.425) - 4.185(\pm 0.523) \times \text{Salinity (psu)}$$

$$(R^2 = 0.37, P < 0.001, n = 52, NRMSE = 17.9\%) \quad (3)$$

3.3. Reproducibility of Ba/Ca_{coral}

While luminescence G/B patterns were cyclical and highly reproducible between all the colonies sampled from the two study sites (Fig. 4a/b) (Tanzil et al., 2016), well-defined intra-annual patterns could not be discerned for Ba/Ca_{coral} and reproducibility between the replicate colonies was very low (Table 2; Fig. 4c/d). Average Ba/Ca_{coral} values were, however, within ±1 SD of one another (Table 1), with two of the three replicate cores at each site demonstrating increases in Ba/Ca_{coral} over time (Fig. 4c/d). The median between-year variances (median $\sigma^2 = 25.94$) in Ba/Ca_{coral} values were much higher compared to its within-year variances (median $\sigma^2 = 2.06$).

3.4. Ba/Ca_{coral} relationship with Ba_{SW}, Ba/Ca_{SW} and luminescence G/B

Of the six replicate colonies, only one (HT-H) showed significant positive Ba/Ca_{coral}–Ba_{SW} ($P < 0.05$, $r = 0.45$) and Ba/Ca_{coral}–Ba/Ca_{SW} ($P < 0.05$, $r = 0.49$) relationships (Table 3; Fig. 5a–d). No clear relationship was found between the paired monthly averaged luminescence G/B and Ba/Ca_{coral} (Table 2): luminescence and Ba/Ca were significantly negatively correlated in two (HT-I and KU-L) of the six colonies, positively correlated in one core (HT-H) and not correlated in the remaining three (HT-G, KU-F, KU-K) (Table 3). The average distribution of Ba (D_{BA}) of all the *Porites lutea* corals was 0.95 ± SD 0.27. The D_{BA} of individual coral colonies were 0.93 ± SD 0.22 for HT-G, 1.16 ± SD 0.26 for HT-H, 0.88 ± SD 0.19 for HT-I, 0.96 ± SD 0.23 for KU-F, 0.70 ± SD 0.20 for KU-K, 1.04 ± SD 0.29 for KU-L.

3.5. Ba/Ca_{coral} relationship with seawater parameters

Pearson's correlation tests between colony-level monthly Ba/Ca_{coral} vs. temperature, salinity, TSS, OSS, ISS, TSD, OSD, ISD and PAR showed significant relationships with multiple parameters (Table 4; Fig. 5e–n). Out of these, only OSS and TSD showed significant unidirectional relationships with Ba/Ca_{coral} for more than half of the colonies analysed (Table 4). However, correlation coefficients were generally weak for both Ba/Ca_{coral} vs. OSS ($|r| = 0.20$–0.66; significant for four colonies) and for Ba/Ca_{coral} vs. TSD ($|r| = 0.05$–0.56; significant for four colonies) (Table 4).

The 5 top-ranked model fits (out of 310 model permutations for each site and all sites) for variations in Ba/Ca_{coral} at each study site and for all sites based on AIC_C are shown in Table 5, along with their respective ΔAIC_C, RMSE (residual mean square error) and NRMSE (normalised RMSE) values and R^2. It should be noted that R^2 for GAMM models such as those used here is hard to correctly quantify due to its complex model structure and is based on likelihood ratio pseudo-R^2 that represents the 'variance explained' by the fixed-effects of the best model (as selected by AIC_C) (Nakagawa and Schielzeth, 2013). Multi-level analyses generally agreed with colony-level results – significant but weak relationships were found with multiple

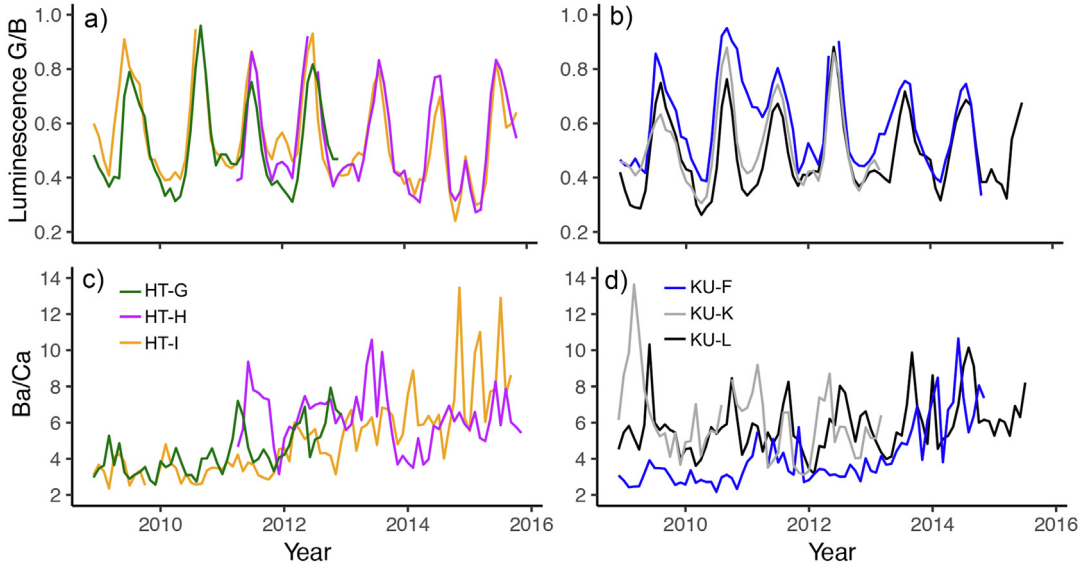

Fig. 4. Monthly-averaged luminescence G/B intensity at (a) P. Hantu and (b) P. Kusu, and Ba/Ca_{coral} at (c) P. Hantu and (d) P. Kusu over the period December 2008–November 2015. HT-G, HT-H, HT-I refer to replicate colonies from P. Hantu; KU-F, KU-K, KU-L refer to replicate colonies from P. Kusu. (For interpretation of the references to colour in this figure legend, the reader is referred to the web version of this article.)

Table 2
Pearson's correlations (r) between Ba/Ca records for replicate colonies from both study sites. Red text = significant negative correlations (i.e. $p < 0.05$); Black text = no significant correlations; df = (number of sample pairs) − 2.

Colony	HT-G	HT-H	HT-I	KU-F	KU-K	KU-L
HT-G	–	r=0.02, p=0.95, df=19	r=0.51, p<0.001, df=47	r=0.05, p=0.72, df=47	r=0.34, p=0.02, df=47	r=0.04, p=0.76, df=47
HT-H	_	_	r=-0.09, p=0.53, df=52	r=0.24, p=0.26, df=22	r=-0.27, p=0.05, df=48	r=0.13, p=0.33, df=50
HT-I	_	_	_	r=-0.03, p=0.85, df=50	r=0.53, p<0.001, df=76	r=0.22, p=0.05, df=78
KU-F	_	_	_	–	r=0.01, p=0.95, df=50	r=0.18, p=0.22, df=50
KU-K	_	_	_	_	_	r=0.17, p=0.13, df=76

parameters (and combinations thereof), with the R^2 for all the top-ranked models ranging from only 0.089–0.16 (Table 5).

At P. Hantu, OSS and PAR were also included in the top-ranked model with the lowest AIC_C, and produced the highest model R^2 of 0.128 and lowest RMSE and NRSME of 1.816 and 16.70 % respectively (Table 5). OSS and PAR also common factors among the top-ranked models, with OSS appearing as a factor in 3 out of the 5 best models, and PAR in 4 out of 5 models (Table 5). Partial effect plots showed that Ba/Ca_{coral} exhibited positive relationships with both OSS and PAR at this site (Fig. 6a/c).

At P. Kusu, the top-ranked model based on lowest AIC_C included TSD, PAR and an interaction term for TSD and salinity (TSD:Sal). This model, however, produced the lowest R^2 of 0.118 among the 5 top-ranked models, with RMSE of 1.390 and NRMSE of 16.38 % (Table 5). The TSD and OSS instead produced the highest model R^2 of 0.160 (NRMSE 16.50 %; ΔAIC_C 3.84), with the TSD + OSS + PAR model producing the second highest R^2 of 0.155 and lowest NRMSE of 15.78% (ΔAIC_C 3.11). TSD

Table 3
Pearson's correlations (r) between Ba/Ca coral and dissolved Ba seawater (Ba_{SW}), seawater Ba/Ca (Ba/Ca_{SW}) and luminescence G/B (G/B). Blue text = significant positive correlation (i.e. $p < 0.05$); Red text = significant negative correlations; Black text = no significant correlations; df = (number of sample pairs) − 2.

Colony	Ba_{SW}	Ba/Ca_{SW}	G/B
HT-G	r=0.21, P=0.44, df=15	r=0.18, P=0.52, df=15	r=-0.14, P=0.35, df=47
HT-H	r=0.39, P=0.06, df=23	r=0.37, P=0.07, df=23	r=0.49, P<0.001, df=54
HT-I	r=0.45, P=0.02, df=25	r=0.49, P=0.01, df=25	r=-0.24, P=0.03, df=80
KU-F	r=0.42, P=0.08, df=16	r=0.37, P=0.15, df=16	r<0.01, P=0.95, df=50
KU-K	r=0.19, P=0.37, df=24	r=0.18, P=0.38, df=24	r=-0.12, P=0.32, df=76
KU-L	r=-0.07, p=0.71, df=24	r<0.01, P=0.98, df=24	r=-0.51, P<0.001, df=78

was a factor in all the top-ranked models for P. Kusu, with PAR included in 3 out of the 5 models. Partial effect plots showed Ba/Ca_{coral} to be positively correlated with OSS (Fig. 6d) and negatively correlated with both TSD and PAR at this study site (Fig. 6e/f).

Multi-level analyses of data from both study sites found the top-ranked model to be an OSS-only model based on lowest AIC_C (Table 5). However, the R^2 was for this univariate model was the lowest at 0.123. The second-ranked OSS and TSD model with ΔAIC_C of 0.53 (i.e. < 2) had the highest model R^2 as well as the lowest NRMSE of 14.54 % (Table 5). OSS was a common factor in 4 out of 5 top-ranked models, while TSD appeared in 2 models.

4. DISCUSSION

4.1. Rivers, salinity and Ba_{SW}

The Johor River, located on the southern tip of mainland Peninsula Malaysia, is the largest river to drain into Singapore waters (Fig. 1). It has an average discharge rate of ~35 $m^3 s^{-1}$ which ranges from ~20 $m^3 s^{-1}$ in July to ~65 $m^3 s^{-1}$ in December (Tanzil et al., 2016). Several small rivers on mainland Singapore with similar seasonal discharge patterns also drain into Singapore waters. However, these have much lower discharges with the area of the largest catchment (Singapore River/Kallang Basin) at only ~20 km^2 (Chia et al., 1988; Lim, 1997; PUB, 2013). Moreover, most rivers on mainland Singapore have been dammed to form reservoirs, including the Singapore River which since 2008 forms the Marina Reservoir (PUB, 2013). Despite peak local rainfall and river discharges occurring during the wetter northeast (NE) monsoon (November–March), salinity minima in Singapore waters are observed during the southwest (SW) monsoon (May–September) when local rainfall and river discharges are lower (Fig. 2c). Alternating monsoon currents in the South China Sea drive this decoupling in the monsoon-related hydrological cycle and salinity in the Singapore Straits. A combination of tidal- and wind-driven currents allow more turbid, lower salinity waters from the Java Sea and/or Malacca Straits to drift/reside longer in the Singapore Straits during the SW monsoon, while flushing clearer, higher salinity waters through the Straits during the NE monsoon (Robinson et al., 1953; Chen et al., 2005; Tanggang et al., 2011; Rizal et al., 2012; Sin et al., 2016; Tanzil et al., 2016).

We found a significant inverse correlation between Ba_{SW} with *in-situ* salinity (Fig. 3). Although this Ba_{SW}–salinity relationship was non-linear, Ba_{SW} concentrations tended to be higher ~ May–September (drier SW monsoon, lowest local river discharge) and lowest ~ October–November (Fig. 2d). This indicates that seasonal Ba variability, as with salinity, in the Singapore Straits is likely driven mainly by sources supplied externally (i.e. from outside of Singapore) rather than by local river discharges or rainfall-related runoff. Non-linearity in the Ba_{SW}–salinity correlation was largely due to the lack of relationship found between Ba_{SW} and lower salinities during the peak SW monsoon months (i.e. June, July, August), which we posit may be due to dilution of a limited Ba supply during this period. The rate of physical and chemical weathering can limit the supply of Ba to tropical rivers, as can sediment exhaustion during successive storm events (Sinclair and McCulloch, 2004; Stock and Tribble, 2010). Strong river outflows can also cause sediment to be deposited in low-salinity waters on the bottom, only released by cation exchange and diffusion when the river flow is weaker and seawater floods the bottom sediments. Intense river discharges during the wet season, in this case experienced by the southwest coast of Peninsula Malaysia during the SW monsoon (Tanzil et al., 2016), could therefore dilute Ba supplies resulting in the decoupling of salinity from Ba_{SW} during this period. For the remaining months (September–May), Ba_{SW} has linear negative correlations with salinity (Fig. 3), the slopes and intercept of which are comparable to those found at the Gulf of Panama (LaVigne et al., 2016). Extrapolating the significant linear regressions of Ba_{SW} and salinity (September–May) back to the approximate salinity of peak dissolved barium concentration in estuaries (~4 psu) yields a dissolved barium concentration of ~160–180 nmol kg^{-1} which is in agreement with an average peak of barium concentrations documented for several estuaries (e.g. Zaire, Amazon, Ganges, Chesapeake and Delaware estuaries) (Edmond et al., 1978; Coffey et al., 1997).

4.2. Ba/Ca_{coral} and seawater measurements

We found very poor replication of the Ba/Ca ratios in the *Porites lutea* cores taken from the same reef site (Table 2, Fig. 4) and only one of the six replicate corals showing a significant but relatively weak positive relationship between coral Ba/Ca and dissolved seawater Ba ($r = 0.45$) (Table 3; Fig. 5a–d). This is in contrast to previous findings by the only other multi-colony calibration study of *Porites* coral Ba/Ca against contemporaneous *in-situ* seawater barium record (LaVigne et al. 2016).

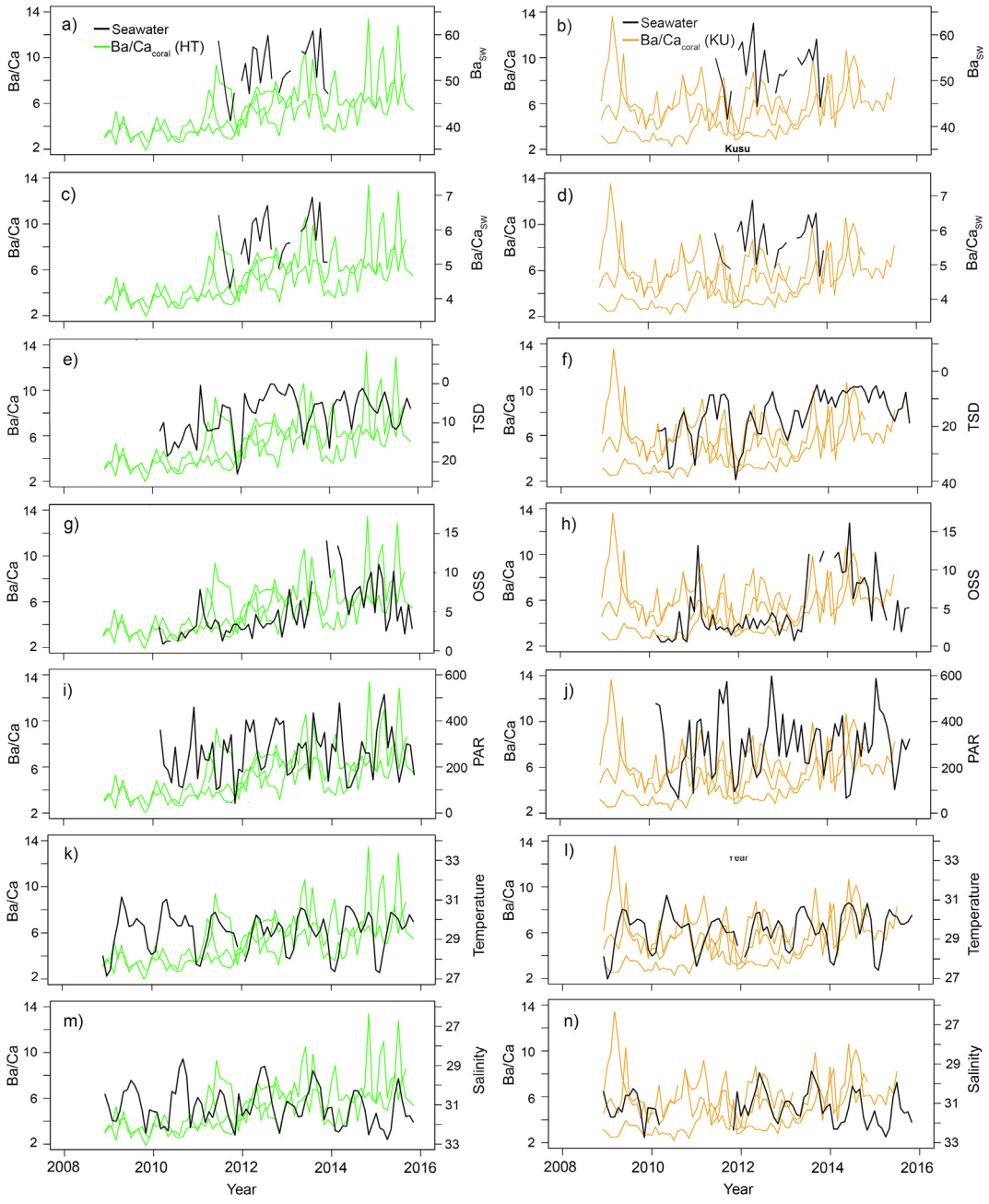

Fig. 5. Plots of Ba/Ca$_{coral}$ from each colony replicate (μmol/mol, coloured lines) and monthly *in-situ* seawater parameters (black lines): (a and b) dissolved barium seawater (Ba$_{SW}$; mol kg^{-1}), (c and d) seawater Ba/Ca (Ba/Ca$_{SW}$; μmol/mol), (e and f) total sedimentation rate (TSD; mg cm^{-2} day^{-1}), (g and h) organic suspended solids (OSS; mg l^{-1}), (i and j) photosynthetically active radiation (PAR; μmol m^{-2} day^{-1}), (k and l) temperature (°C), and (m and n) salinity (psu). (For interpretation of the references to colour in this figure legend, the reader is referred to the web version of this article.)

Lavigne et al. (2016) reported excellent agreement between their three replicate *P. lobata* colonies (Pearson's r = 0.86–0.99) and strong positive linear correlations between their Ba/Ca$_{coral}$ and *in-situ* Ba$_{SW}$ records (Pearson's r = 0.70–0.99). Given that the behaviour of dissolved seawater Ba in the Singapore Straits is in line with findings by LaVigne et al. (2016) for the Gulf of Panama, the lack of relationship found in the current study between Ba/Ca$_{coral}$ and Ba$_{SW}$ or Ba/Ca$_{SW}$ in five out of the six replicate corals, and weak relationship in one core, suggests some other mechanism/s is/are driving the incorporation of Ba into the coral aragonite skeleton, disrupting the equilibrium between coral skeleton and seawater Ba. The relatively wide range of distribution coefficients of Ba (D_{BA}) from 0.70 to 1.16 found for the six *Porites lutea* colonies sampled also support this notion. Furthermore, there was no clear relationship between Ba/Ca$_{coral}$ and luminescence G/B (Table 3, Fig. 4), the latter a coral proxy strongly linked with salinity

Table 4
Results of Pearson's correlation tests between monthly averaged coral Ba/Ca and salinity, temperature, total suspended solids (TSS; mg l^{-1}), inorganic suspended solids (ISS; mg l^{-1}), organic suspended solids (OSS; mg l^{-1}), total sedimentation rate (TSD; mg cm^{-2} day^{-1}), inorganic sedimentation rate (ISD; mg cm^{-2} day^{-1}), organic sedimentation rate (OSD; mg cm^{-2} day^{-1}), and photosynthetically active radiation (PAR; μmol m^{-2} day^{-1}). Blue text = significant positive correlation (i.e. $p < 0.05$); Red text = significant negative correlations; Black text = no significant correlations; df = (number of sample pairs) − 2.

	HT-G	HT-H	HT-I	KU-F	KU-K	KU-L
Salinity	r=0.19, p=0.19, df=47	r=-0.40, p=0.002, df=54	r=0.11, p=0.30, df=80	r=-0.24, p=0.12, df=40	r=0.27, p=0.03, df=66	r=-0.37, p=0.002, df=68
Temperature	r=0.10, p=0.51, df=46	r=0.35, p=0.01, df=53	r=-0.04, p=0.74, df=79	r=-0.08, p=0.60, df=39	r=0.12, p=0.35, df=65	r=0.25, p=0.04, df=67
TSS	r=0.05, p=0.78, df=32	r=-0.32, p=0.02, df=51	r=0.35, p=0.004, df=62	r=0.16, p=0.34, df=34	r=0.31, p=0.02, df=57	r=0.24, p=0.06, df=58
OSS	r=0.32, p=0.06, df=32	r=-0.21, p=0.13, df=51	r=0.46, p<0.001, df=62	r=0.20, p=0.24, df=34	r=0.66, p<0.001, df=57	r=0.26, p=0.04, df=58
ISS	r=-0.05, p=0.79, df=32	r=-0.33, p=0.01, df=51	r=0.29, p=0.02, df=34	r=0.09, p=0.61, df=57	r=0.54, p<0.001, df=57	r=0.24, p=0.07, df=58
TSD	r=-0.56, p<0.001, df=32	r=-0.05, p=0.70, df=54	r=-0.25, p=0.04, df=65	r=-0.09, p=0.59, df=35	r=-0.46, p<0.001, df=61	r=-0.44, p<0.001, df=63
OSD	r=-0.64, p<0.001, df=14	r=-0.02, p=0.9, df=49	r=0.08, p=0.60, df=47	r=-0.37, p=0.11, df=17	r=-0.43, p=0.007, df=37	r=-0.42, p=0.003, df=45
ISD	r=-0.56, p=0.02, df=14	r=-0.09, p=0.52, df=49	r=0.05, p=0.73, df=47	r=-0.31, p=0.19, df=17	r=-0.58, p<0.001, df=37	r=-0.45, p=0.001, df=45
PAR	r=0.51, p=0.002, df=32	r=0.11, p=0.40, df=54	r=0.17, p=0.15, df=65	r<0.01, p=0.98, df=35	r=0.02, p=0.88, df=61	r=-0.12, p=0.33, df=63

Table 5
Best 5 linear mixed effects (LME) models (out of a total of 310 tested heuristically) based on AIC_C and their respective Δ (difference from lowest model AIC_C value), log-likelihood R^2, residual mean square error (RMSE) and normalised residual mean square error (NRMSE) for coral Ba/Ca at each of the study sites, P. Hantu (HT) and P. Kusu (KU), and for all sites (All).

Site	Model	AICc	ΔAICc	R^2	RMSE	NRMSE (%)
HT	OSS + PAR	547.81	–	0.128	1.816	16.67
	PAR	547.96	0.15	0.089	1.838	16.87
	PAR + PAR:OSS	549.08	1.27	0.121	1.865	17.13
	Temp + PAR	550.48	2.67	0.100	1.819	16.70
	OSS	550.96	3.15	0.123	1.859	17.06
KU	TSD + PAR + TSD:Sal	551.16	–	0.118	1.390	16.38
	TSD + PAR	552.20	1.04	0.120	1.376	16.22
	TSD	553.20	2.04	0.125	1.470	17.32
	TSD + OSS + PAR	554.27	3.11	0.155	1.339	15.78
	TSD + OSS	555.00	3.84	0.160	1.400	16.50
All	OSS	949.10	–	0.123	1.686	14.93
	OSS + TSD	949.63	0.53	0.160	1.643	14.54
	OSS + PAR:Temp	949.87	0.77	0.125	1.683	14.90
	TSD	950.53	1.42	0.125	1.692	14.98
	Temp + OSS	951.43	2.33	0.142	1.663	14.73

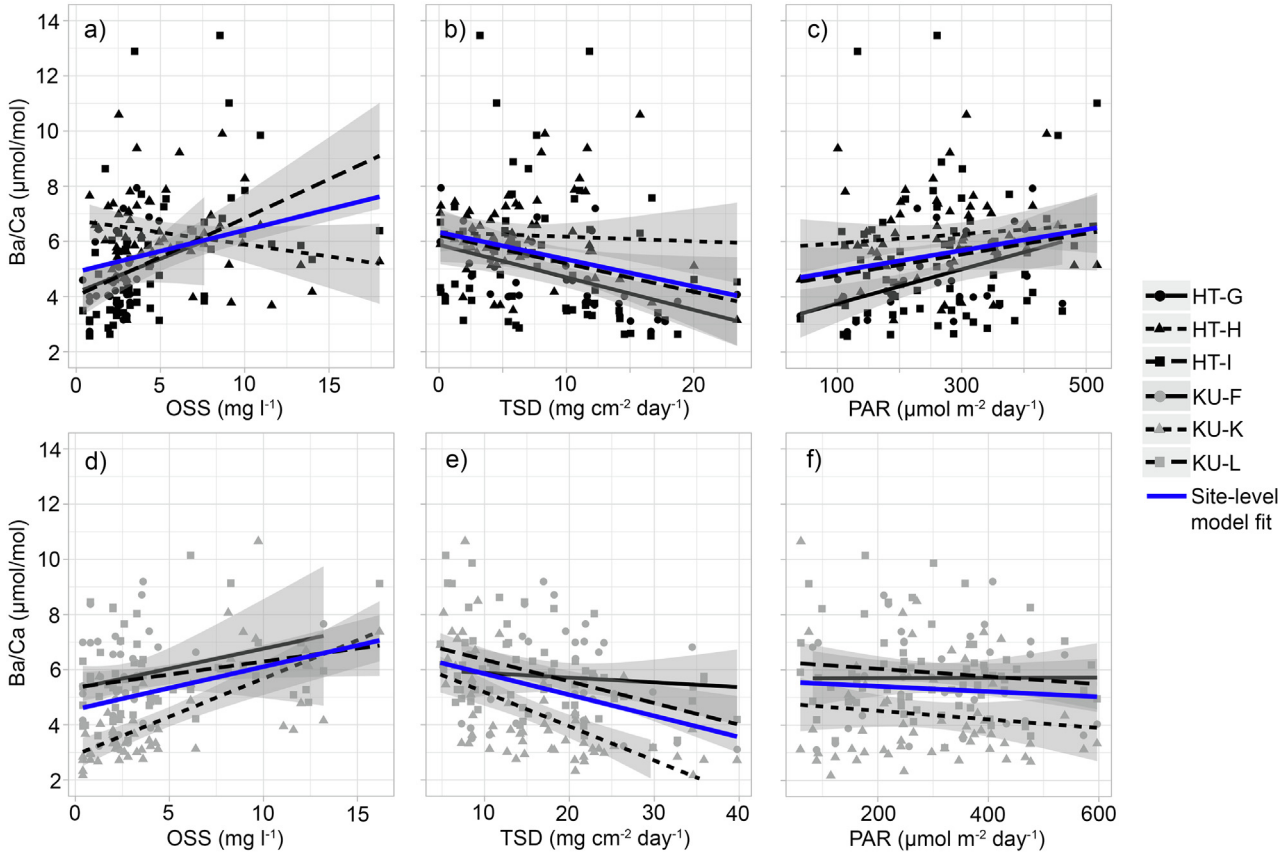

Fig. 6. Partial effects plot showing relationships between Ba/ Ca_{coral} and organic suspended solids (OSS), total sedimentation rate (TSD) and photosynthetically active radiation (PAR) at P. Hantu (a–c) and P. Kusu (d–f) for replicate corals (black lines) and at the site-level (blue lines). Gray shaded area denote 95% confidence interval of the model. (For interpretation of the references to colour in this figure legend, the reader is referred to the web version of this article.)

and river runoff and highly reproducible across replicate colonies (Fig. 4) (Isdale, 1984; Lough, 2007; Jupiter et al, 2008; Lough et al., 2015; Tanzil et al. 2016). This not only implies that the incorporation of dissolved terrestrially derived humic-like substances into the coral is independent of Ba, but also that factors aside from freshwater discharge/flood events are driving the poor inter-colony replication of Ba/Ca and disconnect with Ba_{SW} found in the present study.

Lewis et al. (2018) found similar poor replication in Ba/Ca_{coral} recorded by duplicate corals sampled from the same location at the Great Barrier Reef (GBR). Of the ten corals from five locations analysed, only four showed significant positive correlations with luminescence and regional river discharge (Lewis et al., 2018). While the authors did not go into detail of the potential causes of such perplexing behaviour, they did postulate possible influence from their sodium hypochlorite (NaOCl) cleaning treatment i.e. a method developed by Nagtegaal et al. (2012) that was shown to effectively remove non-skeletal barite spikes. The authors suggested that during the NaOCl treatment, the organic tissue layer instead of being flushed from the coral piece in the cleaning process was somewhat mobilized, redistributed and trapped throughout the piece in some instances but not others. Although the present study also treated all corals with NaOCl cleaning prior to analyses, it is unlikely that the inter- and intra-colony variability in Ba/Ca_{coral} found here resulted from non-skeletal Ba inclusions, including contamination by redistributed tissue layer. Further testing of NaOCl only treatment vs. NaOCl followed by a more rigorous secondary cleaning sequence as per Shen and Boyle (1988) yielded highly comparable Ba/Ca results on paired samples from two different corals (Fig. S1).

Aside from non-skeletal Ba-rich contaminants, a number of other possibilities put forward as potential causes of variability in coastal Ba/Ca_{coral} include: (1) Ba-enrichment associated with coastal upwelling (Tudhope et al., 1996), (2) barite formation associated with phytoplankton blooms and decays (Sinclair, 2005; Gilikin et al., 2006), (3) seasonal variations related to sea temperatures (Fallon, et al. 2003; Grove et al., 2012), (4) Ba release associated with sediment fluxes (sources, storage and resuspension) (Prouty et al., 2010; Stock and Tribble, 2010), (5) uptake of barite-rich particles through ingestion (Stecher and Kogut, 1999; Sinclair, 2005; Gilikin et al., 2006), and (6) incorporation of metals into skeletons as mediated by other biological factors (Brown et al., 1991;

Allison et al., 2018). As Singapore does not experience upwelling events (due to its location on the inner continental Sunda shelf in shallow waters < 30 m), and no anomalous phytoplankton blooms were observed in the Singapore Straits during the 2008–2015 study period, possible causes (1) and (2) outlined above can be ruled out. The remaining possible causes of Ba/Ca variability are discussed below.

4.3. Variations in sea temperature

The current study found relatively weak relationships between Ba/Ca_{coral} and several monthly *in-situ* seawater parameters, including temperature (Tables 4 and 5, Fig. 5). Previous studies have shown that sea temperature is a known driver of thermodynamically regulated incorporation of cations in marine carbonates and that Ba incorporation into coral aragonite is inversely affected by temperature (Hart and Cohen, 1996; Cohen and McConnaughey, 2003). Our data, however, reveal the opposite tendency if any, i.e. positive relationship between Ba/Ca_{coral} and temperature (Table 4; Fig. 5). Hence it is unlikely that temperature is a significant driver of coral Ba/Ca variability found in the current study. LaVigne et al. (2016) also noted positive Ba/Ca_{coral}–temperature relationships for their Panama coral records, and concluded similarly.

4.4. Sediment fluxes

Out of a total of nine contemporaneous seawater parameters tested against Ba/Ca_{coral}, organic suspended sediments (OSS) and total sedimentation rate (TSD) appeared to be common factors among the replicate colonies (Table 4) as well as among the top-ranked models identified through multi-level analyses (Table 5). Although the R^2 of the OSS and/or TSD liner mixed-effects (LME) models identified are weak (maximum $R^2 = 0.16$), the repeat inclusion of these factors in the top-ranked models suggests that OSS and TSD – both sediment flux-related parameters – are likely important factors driving coral Ba/Ca within the current dataset (Tables 4 and 5, Fig. 5). Previous studies have suggested that post-deposition processes, such as re-suspension, could be driving coral Ba/Ca variability by promoting Ba desorption from particles which serve as an added source of dissolved Ba for coral incorporation (Esslemont et al., 2004; Sinclair, 2005; Prouty et al., 2010). Although Singapore is sheltered from strong winds (maximum wind speeds of $<3\ m\ s^{-1}$) and does not experience large waves (maximum wave height typically ~ 1 m), the Singapore Straits is one the world's busiest shipping lanes. Regular ship and boat traffic in the Singapore Straits create large wakes that can trigger high frequency (hourly–daily) re-suspension of sediment on Singapore's shallow reefs (Shue, 2017). Within a horizontal traverse of l00 m, or less on some reefs, marked variations in the topography, wave action, current speed, irradiance and sedimentation pattern can exist (Done, 1983; Brown, 1997). Within-reef spatio-temporal heterogeneity in re-suspension or sediment-desorbed Ba may therefore be driving the inter-colony variability in Ba/Ca_{coral} and weak/lack of relationship between Ba/Ca_{coral} and Ba_{SW}. While the present study found no significant relationship between monthly sampled Ba_{SW} and either OSS ($r = 0.14$, $P = 0.07$) or TSD ($r = 0.09$, $P = 0.23$), there is the possibility that once monthly spot sampling/measurement may be insufficient to capture and calibrate any relationships between Ba_{SW}, on-reef sediment fluxes and Ba/Ca_{coral}. It is also possible that the concentration of Ba in particulates as well as dissolved in seawater may need to be accounted for. Interestingly, when the bivariate OSS + TSD model was applied to 1-year binned averages of Ba/Ca_{coral}, we found improved log-likelihood R^2 of 0.41 for P. Hantu (RMSE = 1.06; NRMSE = 19.0%), of 0.76 for P. Kusu (RMSE = 0.56; NRMSE = 12.3%), and of 0.49 for all sites (RMSE = 0.90; NRMSE = 15.6%). This could indicate potential for Ba/Ca_{coral} as a proxy for reconstructing inter-annual variability of sediment-related flux, or closely related parameters, in Singapore reef waters.

4.5. Ingestion of Ba-rich particulates

Although no direct link between ingestion by coral of Ba-rich particles and coral skeletal Ba/Ca have been shown, peaks in Ba/Ca observed in some bivalves have previously been attributed to ingestion and uptake of barite-rich particles (Stecher et al. 1996; Putten et al. 2000; Gilikin et al. 2006). Hermatypic corals, such as *Porites lutea*, used in the current study are essentially polytrophic. While the majority of the time they are autotrophic obtaining energy via their photosynthetic endosymbiont, they are also heterotrophic and known to feed not only on plankton but also other suspended solids including sediments and even microplastics (Sebens et al., 1996; Anthony and Fabricius, 2000; Anthony, 2000; Houlbrèque et al., 2004; Hall et al., 2015). As feeding efforts and rates can vary between coral individuals of the same species (e.g. Ferrier-Pagès et al., 2010), Ba-enrichment through feeding could account for the high inter-colony variability in Ba/Ca_{coral} found in the present study (Table 2, Fig. 4) and in Lewis et al. (2018) that contrast the inter-colony reproducibility reported in LaVigne et al. (2016). Corals analysed in LaVigne et al. (2016) were sampled from a much clearer water location (Playa Cacique, Isla Contadora, Gulf of Panama) and are presumably predominately autotrophic. Conversely, Singapore's corals exist in a highly urbanised and dynamic coastal environment that is subject to elevated sedimentation, suspended sediments, turbidity, and depressed light penetration (Tun et al., 1994; Dikou and van Woesik, 2006; Sin et al. 2016). Tun et al. (1994) found that at ~3 m water depth, Singapore's corals are barely meeting their daily carbon requirements solely from photosynthesis and are likely supplementing their energetic needs via increased heterotrophy. Corals on Singapore's sediment-rich reefs may therefore be ingesting sizable amounts of Ba-rich particles in the water column, allowing for increased Ba to be incorporated into their skeletons. A similar mechanism may be contributing to the inter-colony variability in Ba/Ca_{coral} also seen in Lewis et al. (2018). Corals analysed by Lewis et al. (2018) were sampled from sites that can be constituted as inshore reefs located within the boundary of the terrigenous sediment wedge (Anthony,

2000). Corals from these sites were found to have particle feeding rates up to 4 times of conspecifics from less turbid, midshelf reefs. Enrichment through feeding mechanisms could therefore likely explain the positive relationship between suspended solids and Ba/Ca_{coral} in our dataset (Tables 4 and 5), as well as the inverse correlation between Ba/Ca_{coral} and sedimentation rate (TSD) i.e. higher downward sediment flux results in increased sediment deposition onto corals or smothering, suppressing the ability of corals to feed (Junjie et al., 2014). In addition to sediment-flux parameters, PAR also appeared as a common factor in the top-ranked site-level models. PAR plays a role in defining coral trophic dynamics, and hence feeding efforts (e.g. Anthony, 2000). However, the relationship between Ba/Ca_{coral} and PAR were ultimately noisy, and not consistent across sites (Fig. 6c/f). Further investigation is required to validate the hypotheses proposed here, especially considering the low model fits and complex nature of relationships found between Ba/Ca_{coral} and the contemporaneous *in-situ* seawater variables.

4.6. Incorporation of Ba mediated by other biological factors

Allison et al. (2018) found massive adult *Porites* spp. corals of the same species incorporated widely varying skeletal Ba/Ca (2–3 fold differences in their D_{BA}) under the same culture conditions. Variations in D_{BA} found were not correlated with coral photosynthesis, respiration or calcification rates but were associated with different genotypes (Allison et al., 2018). While it is yet unresolved how within-species genotype variations affect mechanisms of Ba incorporation, it is highly plausible that genotypic differences could be driving the inter-colony variability in *Porites lutea* Ba/Ca found in the current study. The current study found no relationship between average calcification rates and D_{BA} ($P = 0.51$, $r = 0.33$). It is, however, possible that Ba could also be associated with a non-aragonite phase and the proportion and composition (if organic) of which may affect skeletal Ba/Ca incorporation (Allison et al., 2018). Other possible biological/behavioural mechanisms by which corals could potentially mediate incorporation of trace elements into their skeletons include tissue-retraction behaviour (Brown et al., 1991), coral mucus and muco-ciliary feeding (Lewis, 1977; Goldberg, 2002; Brown and Bythell, 2005).

4.7. Conclusion

To summarise, we found from Singapore's turbid urban reefs high inter-colony variability in Ba/Ca_{coral} and weak to no relationship between Ba/Ca_{coral} and dissolved seawater Ba that contradicts a previous multi-colony calibration study by LaVigne et al. (2016) in an open ocean environment. We also found no clear link between Ba/Ca_{coral} and coral luminescence G/B which suggest that Ba/Ca_{coral} in Singapore is unlikely to be driven by the same riverine discharge/runoff processes as skeletal luminescence. The current study represents the first to assess the relationship coral between Ba/Ca as well as years-long monthly-resolution contemporaneous measurements of *in-situ* seawater parameters (temperature, salinity, suspended sediments, sedimentation rate and photosynthetically active radiation). Our results suggest that reef sediment flux, coral feeding and/or other behavioural responses to the environment may be driving the highly variable nature of Ba/Ca_{coral} in our dataset. However, the model fits that were found are relatively weak (Tables 4 and 5) suggesting that Ba/Ca on its own is an incomplete proxy, and likely very site specific. Incorporation into coral aragonite may be more complex than previously thought – with possible contributions from as-yet unaccounted aspects of Ba biogeochemical cycling, or coral biological factors, or a combination of both. While further studies are needed to tease apart the effects of these potential drivers, our results highlight the need for careful selection and replicated approaches in order to avoid conflicting interpretations and to obtain more accurate and precise reconstructions from coral Ba/Ca as a proxy. Additional work is required to quantify direct links between Ba incorporated into coral skeleton and particulates/sediment and coral food sources, e.g. using Ba isotopes (Hsieh and Henderson, 2017), which will likely lead to a better understanding of the Ba biogeochemical cycling along with more reliable and potentially broader applications of the coral Ba/Ca proxy.

ACKNOWLEDGEMENTS

This paper is dedicated to the memory of our colleague, friend and mentor, Dr. Sin Tsai Min (1970–2017). Many thanks to the Singapore National Parks for allowing us to conduct this research (permit no. NP/RP16-156-1). Thanks also to Miss Rosabelle Ong for her assistance in the lab and in the field. Funding was provided by the Singapore National Research Foundation (NRF), Prime Minister's Office, under the Marine Science Research and Development Programme (Project MSRDP-03 "Adaptation and resilience of coral reefs to environmental change in Singapore"). We also thank the NRF for the St. John's Island National Marine Laboratory. A portion of the research described in this project was funded by the NRF through the Singapore-MIT Alliance for Research and Technology (SMART) Center for Environmental Sensing and Modeling (CENSAM) and by the Singapore Ministry of Education under the Research Centres of Excellence initiative (Grant Number M4430139). We thank the Public Utilities Board (PUB), Singapore, for granting us the use of their long-term marine water quality monitoring data.

APPENDIX A. SUPPLEMENTARY MATERIAL

Supplementary data to this article can be found online at https://doi.org/10.1016/j.gca.2019.01.034.

REFERENCES

Alibert C. and McCulloch M. (1997) Strontium/calcium ratios in modern *Porites* corals From the Great Barrier Reef as a proxy for sea surface temperature: calibration of the thermometer and monitoring of ENSO. *Paleoceanography* **12**, 345–363.

Alibert C., Kinsley L., Fallon S. J., McCulloch M. T., Berkelmans R. and McAllister F. (2003) Sources of trace element variability in Great Barrier Reef corals affected by the Burdekin flood plumes. *Geochim. Cosmochim. Acta* **67**, 231–246.

Allison N., Cole C., Hintz C., Hintz K. and Finch A. A. (2018) Influences of coral genotype and seawater pCO_2 on skeletal Ba/

Ca and Mg/Ca in cultured massive *Porites* spp. corals. *Palaeogeogr. Palaeoclimatol. Palaeoecol.* **505**, 351–358.

Anthony K. (2000) Enhanced particle-feeding capacity of corals on turbid reefs (Great Barrier Reef, Australia). *Coral Reefs* **19**, 59–67.

Anthony K. R. N. and Fabricius K. (2000) Shifting roles of heterotrophy and autotrophy in coral energetics under varying turbidity. *J. Exp. Mar. Biol. Ecol.* **252**, 221–253.

Bartoń, K. (2013) MuMIn: Multi-model inference. R package version 2013.

Bird M. I., Pang W. C. and Lambeck K. (2006) The age and origin of the Straits of Singapore. *Palaeogeogr. Palaeoclimatol. Palaeoecol.* **241**, 531–538.

Bolton A., Goodkin N. F., Hughen K., Ostermann D. R., Vo S. T. and Phan H. K. (2014) Paired *Porites* coral Sr/Ca and $\delta^{18}O$ from the western South China Sea: Proxy calibration of sea surface temperature and precipitation. *Palaeogeogr. Palaeoclimatol. Palaeoecol.* **410**, 233–243.

Boto K. and Isdale P. J. (1985) Fluorescent bands in massive corals result from terrestrial fulvic acid inputs to nearshore zone. *Nature* **315**, 396–397.

Brenner L. D., Linsley B. K. and Dunbar R. B. (2017) Examining the utility of coral Ba/Ca as a proxy for river discharge and hydroclimate variability at Coiba Island, Gulf of Chirquí, Panamá. *Mar. Pollut. Bulleting* **118**, 48–56.

Brown B. E. (1997) Adaptations of reef corals to physical environmental stress. *Adv. Mar. Biol.* **31**, 221–299.

Brown B. E. and Bythell J. C. (2005) Perspectives on mucus secretion in reef corals. *Mar. Ecol. Progr. Series* **296**, 291–309.

Brown B. E., Tudhope A. W., Le-Tissier M. D. A. and Scoffin T. P. (1991) A novel mechanism for iron incorporation into coral skeletons. *Coral Reefs* **10**, 211–215.

Burke L., Selig E. and Spalding M. (2002) Reefs at risk in Southeast Asia. World Resources Institute, Washington.

Calcagno V. and Mazancourt C. (2010) glmulti: an R package for easy automated model selection with (generalized) linear models. *J. Statist. Software* **34**, 1–29.

Carriquiry J. D. and Horta-Puga G. (2010) The Ba/Ca record of corals from the Southern Gulf of Mexico: contributions from land-use changes, fluvial discharge and oil-drilling muds. *Mar. Pollut. Bull.* **60**, 1625–1630.

Chen M. L., Lee J.-M., Nurhati I. S., Switzer A. D. and Boyle E. A. (2015) Isotopic record of lead in Singapore Straits during the last 50 years: spatial and temporal variations. *Mar. Chem.* **168**, 49–59.

Chen M., Murali K., Khoo B.-C., Lou J. and Kumar K. (2005) Circulation modeling in the Strait of Singapore. *J. Coastal Res.* **21**, 960–972.

Chia L. S., Khan H and Chou L. M. (1988) The Coastal Environmental Profile of Singapore. Singapore, ASEAN, USCRMP.

Coffey M., Dehairs F., Collette O., Luther G., Church T. and Jickells T. (1997) The behaviour of dissolved barium in estuaries. *Estuarine Coastal Shelf Sci.* **45**, 113–121.

Cohen A. L. and McConnaughey T. A. (2003) Geochemical perspectives on coral mineralization. *Rev. Mineral. Geochem.* **54**, 151–187.

Dickens G. R., Fewless T., Thomas E. and Bralower T. J. (2003) Excess barite accumulation during the Paleocene/Eocene thermal maximum: massive input of dissolved barium from seafloor gas hydrate reservoirs. Causes and Consequences of Globally Warm Climates in the Early Paleogene. *Geol. Soc. Am. Spec. Publ.* **369**, 11–23.

Dietzel M., Gussone N. and Eisenhauer A. (2004) Co-precipitation of Sr^{2+} and Ba^{2+} with aragonite by membrane diffusion of CO_2 between 10 and 50 °C. *Chem. Geol.* **203**, 139–151.

Dikou A. and van Woesik R. (2006) Survival under chronic stress from sediment load: spatial patterns of hard coral communities in the southern islands of Singapore. *Mar. Pollut. Bull.* **52**, 7–21.

Done T. J. (1983) Coral zonation: its nature and significance. In *Perspectives on Coral Reefs* (ed. D. J. Barnes). Australian Institute of Marine Science, Brian Clouston, Manuka.

Dymond J., Suess E. and Lyle M. (1992) Barium in deep-sea sediment: a geochemical proxy for paleoproductivity. *Paleoceanography* **7**, 163–181.

Edmond J. M., Boyle E. D., Drummond D., Grant B. and Mislick T. (1978) Desorption of barium in the plume of the Zaire (Congo) river. *Neth. J. Sea Re.* **12**, 324–328.

Esslemont G., Russle R. A. and Maher W. A. (2004) Coral record of harbour dredging: Townsville, Australia. *J. Mar. Syst.* **52**, 51–64.

Fallon S. J., McCulloch M. T. and Alibert C. (2003) Examining water temperature proxies in Porites corals from the Great Barrier Reef: a cross-shelf comparison. *Coral Reefs* **22**, 309–404.

Ferrier-Pagès C., Rottier C., Beraud E. and Levy O. (2010) Experimental assessment of the feeding effort of three scleractinian coral species during a thermal stress: effect on the rates of photosynthesis. *J. Exp. Mar. Biol. Ecol.* **390**, 118–124.

Fleitmann D., Dunbar R. B., McCulloch M., Mudelsee M., Vuille M., McClanahan T. R., Cole J. E. and Eggins S. (2007) East African soil erosion recorded in a 300 year old coral colony from Kenya. *Geophys. Res. Lett.* **34**, L04401.

Gilikin D. P., Dehairs F., Lorrain A., Steenmans D., Baeyens W. and Andre L. (2006) Barium uptake into the shells of the common mussel (*Mytilus edulis*) and the potential for estuarine paleo-chemistry reconstruction. *Geochimica et Cosmochimica Acta* **70**, 395–407.

Goh N. K. C. and Chou L. M. (1993) The coral reef community of Pulau Satumu (Raffles Lighthouse), Singapore, with emphasis on the hard corals. *J. Singapore Natl Acad. Sci.* **20–21**, 51–57.

Goldberg W. M. (2002) Feeding behaviour, epidermal structure and mucus cytochemistry of the scleractinian Mycetophy*llis reesi*, a coral without tentacles. *Tissue Cell* **34**, 232–245.

Goldstein S. J. and Jacobsen S. B. (1988) Nd and Sr isotopic systematics of river water suspended material – implications for crustal evolution. *Earth Planet. Sci. Lett.* **87**, 249–265.

Goodkin N. F., Hughen K. A., Cohen A. L. and Smit S. R. (2005) Record of Little Ice Age sea surface temperatures at Bermuda using a growth-dependent calibration of coral Sr/Ca. *Paleoceanography* **20**. https://doi.org/10.1029/2005PA001140.

Grove C. A., Zinke J., Scheufen T., Maina J., Epping E., Boer W., Randriamanantsoa B. and Brummer G. J. A. (2012) Spatial linkages between coral proxies of terrestrial runoff across a large embayment in Madagascar. *Biogeosciences* **9**, 3063–3081.

Grove C. A., Nagtegaal R., Zinke J., Scheufen T., Koster B., Kasper S., McCulloch M., van der Bergh G. and Brummer G. J. A. (2010) River runoff reconstructions from novel spectral luminescence scanning of massive coral skeletons. *Coral Reefs* **29**, 579–591.

Guest J. R., Low J., Tun K., Wilson B., Ng C., Raingeard D., Ulstrup K. E., Tanzil J. T. I., Todd P. A., Toh T. C., McDougald D., Chou L. M. and Steinberg P. D. (2016) Coral community response to bleaching on a highly disturbed reef. *Scientific Reports* **6**, 20717.

Hall N. M., Berry K. L. E., Rintoul L. and Hoogenboom M. O. (2015) Microplastic ingestion by scleractinian corals. *Mar. Biol.* **162**, 725–732.

Hanor J. S. and Chan L. H. (1977) Non-conservative behaviour of barium during mixing of Mississippi River and Gulf of Mexico waters. *Earth Planet. Sci. Lett.* **37**, 242–250.

Hart S. R. and Cohen A. L. (1996) An ion probe study of annual cycles of Sr/Ca and other trace elements in corals. *Geochim. Cosmochim. Acta* **60**, 3075–3084.

Houlbrèque F., Tambutte E., Allemand D. and Ferrier-Pagès C. (2004) Interactions between zooplankton feeding, photosynthesis and skeletal growth of the scleractinian coral Stylophora pistillata. *J. Experiment. Biol.* **207**, 1461–1469.

Hsieh Y.-T. and Henderson G. M. (2017) Barium stable isotopes in the global ocean: Tracer of Ba inputs and utilization. *Earth Planet. Sci. Lett.* **473**, 269–278.

Hutchinson C. S. and Tan D. K. (2009) Geology of Peninsular Malaysia. University of Malaya, Malaysia.

Isdale P. J. (1984) Fluorescent bands in massive corals record centuries of coastal rainfall. *Nature* **310**, 578–579.

James G., Witten D., Hastie T. and Tibshirani R. (2013) An Introduction to Statistical Learning. Springer, New York.

Junjie R. K., Browne N. K., Erftemeier P. L. A. and Todd P. A. (2014) Impacts of sediments on coral energetics: partitioning effects of turbidity and settling particles. *PLoS ONE* **9**, e107195.

Jupiter S., Roff G., Marion G., Henderson M., Schrameyer V., McCulloch M. and Hoegh-Guldberg O. (2008) Linkages between coral assemblages and coral proxies of terrestrial exposure along a cross-shelf gradient on the southern Great Barrier Reef. *Coral Reefs* **27**, 887–903.

Koh T. and Lin J. (2006) The land reclamation case: thoughts and reflections. *Singapore Year Book of International Law and Contributors (SYBIL)* **10**, 1–7.

LaVigne M., Grottoli A. G., Palardy J. E. and Sherrell R. M. (2016) Multi-colony calibrations of coral Ba/Ca with a contemporaneous in situ seawater barium record. *Geochimica et Cosmochimica Acta* **179**, 203–216.

LaVigne M., Hill T. M., Spero H. J. and Guilderson T. P. (2011) Bamboo coral Ba/Ca: calibration of a new deep ocean refractory nutrient proxy. *Earth Planet. Sci. Lett.* **312**, 506–515.

Lea D. W. and Spero H. J. (1992) Experimental determination of barium uptake in shells of the planktonic foraminifera Orbulina universa at 22 C. *Geochim. Cosmochim. Acta* **56**, 2673–2680.

Lea D. W., Shen G. T. and Boyle E. A. (1989) Coralline barium records temporal variability in equatorial Pacific upwelling. *Nature* **340**, 373–376.

Leng C. B. and Lim G. S. Y. (1990). An assessment of a patch reef community west of Pulau Hantu. In Coastal Living Resources of Singapore: Proceedings of a Symposium on the Assessment of Living Resources in the Coastal Areas of Singapore (ed. L. M. Chou). National University of Singapore, Singapore. pp. 117–124.

Lewis J. B. (1977) Suspension feeding in Atlantic reef corals and the importance of suspended particulate matter as a food source. Proceedings of the 3rd International Coral Reef Symposium 1, 405–408.

Lewis S. E., Lough J. M., Cantin N. E., Matson E. G., Kinsley L., Bainbridge Z. T. and Brodie J. E. (2018) A critical evaluation of coral Ba/Ca, Mn/Ca and Y/Ca ratios as indicators of terrestrial input: new data from the Great Barrier Reef, Australia. *Geochimica et Cosmochimica Acta* **237**, 131–154.

Lim M. C. (1997) Drainage planning and control in the urban environment the Singapore experience. *Environ. Monit. Assess.* **44**, 183–197.

Llewellyn L. E., Everingham Y. L. and Lough J. M. (2012) Pharmacokinetic modeling of multi-decadal lumiscence time series in coral skeletons. *Geochim. Cosmochim. Acta* **83**, 263–271.

Lough J. M., Cantin N. E., Benthuysen J. A. and Cooper T. F. (2015) Environmental drivers of growth in massive *Porites* corals over 16 degrees latitude along Australia's northwest shelf. *Limnol. Oceanogr.* **61**, 684–700.

Lough J. M. (2010) Climate records from corals. *WIREs Climate Change* **1**, 318–331.

Lough J. M. (2007) Tropical river flow and rainfall reconstructions from coral luminescence: Great Barrier Reef, Australia. *Paleoceanography* **22**, PA2218.

Low J. K. Y. and Chou L. M. (1994) Coral reef fish communities in a sediment stressed environment. Proceedings of the fourth LIPI-JSPS Joint Seminar on Marine Science, 91–99.

Lu X. X., Wong P. P. and Chou L. M. (2005) Singapore's biophysical environment. McGraw-Hill Education, Asia.

Maina J., de Moel H., Vermaat J. E., Henrich-Bruggemann J., Guillaume M. M., Grove C. A., Madin J. S., Mertz-Kraus R. and Zinke J. (2012) Linking coral river runoff proxies with climate variability, hydrology and land-use in Madagascar catchments. *Mar. Pollut. Bullet.* **64**, 2047–2059.

Marshall J. F. and McCulloch M. (2002) An assessment of the Sr/Ca ratio in shallow water hermatypic corals as a proxy for sea surface temperature. *Geochimica et Cosmochimica Acta* **66**, 3263–3280.

McCulloch M., Fallon S., Wyndham T., Hendy E., Lough J. M. and Barnes D. (2003) Coral record of increased sediment flux to the inner Great Barrier Reef since European settlement. *Nature* **421**, 727–730.

Moyer R. P., Grottoli A. G. and Olesik J. W. (2012) A multiproxy record of terrestrial inputs to the coastal ocean using minor and trace elements (Ba/Ca, Mn/Ca, Y/Ca) and carbon isotopes (δ13C, Δ14C) in a nearshore coral from Puerto Rico. *Paleoceanography* **27**. https://doi.org/10.1029/2011PA002249.

Muggeo V. M. R. (2008) Segmented: an R package to fit regression models with broken-line relationships. *R News* **8**(1), 20–25.

Montaggioni L. F., Le Cornec F., Corrége T. and Cabioch G. (2006) Coral barium/calcium record of mid-Holocene upwelling activity in New Caledonia, South-West Pacific. *Palaeogeogr. Palaeoclimatol. Palaeoecol.* **237**, 436–455.

Nakagawa S. and Schielzeth H. (2013) A general and simple method for obtaining R^2 from generalized linear mixed-effects models. *Method Ecol. Evolut.* **4**, 133–142.

Nagtegaal R., Grove C. A., Kasper S., Zinke J., Boer W. G. and Brummer J. A. (2012) Spectral luminescence and geochemistry of coral aragonite: effects of whole-core treatment. *Chem. Geol.* **318–319**, 6–15.

Nicholls R. J., Wong P. P., Burkett V. R., Codignotto J. O., Hay J. E., McLean R., Ragoonaden S. and Woodroffe D. (2007) Coastal systems and low-lying areas. In *Climate change 2007: Impacts, adaptation and vulnerability Contribution of working group II to the fourth assessment report of the Intergovernmental Panel on Climate Change* (eds. M. L. Parry, O. F. Canziani, J. P. Palutikof, P. J. van der Linden and C. E. Hanson). Cambridge University, Cambridge, pp. 315–356.

Paillard D., Labeyrie L. and Yiou P. (1996) Macintosh Program performs time-series analysis. *Eos Trans. Am. Geophys. Union* **77**, 379.

Paytan A. and Kastner M. (1996) Benthic Ba fluxes in the central Equatorial Pacific, implications for the oceanic Ba cycle. *Earth Planet. Sci. Lett.* **142**, 439–450.

Pinheiro J. C. and Bates D. M. (2000) Mixed-Effects Models in S and S-PLUS. Springer, New York.

Pinheiro J., Bates D., DebRoy S., Sarkar D. and R Core Team (2017) nlme: Linear and Nonlinear Mixed Effects Models. R package version 3.1-131 <https://CRAN.R-project.org/package=nlme>.

Prouty N. G., Field M. E., Stock J. D., Jupiter S. D. and McCulloch M. (2010) Coral Ba/Ca records of sediment input to the fringing reef of the southshore of Moloka'i, Hawai'i over the last several decades. *Mar. Pollut. Bullet.* **60**, 1822–1835.

Prouty N. G., Storlazzi C. D., McCutcheon A. L. and Jenson J. W. (2014) Historic impact of watershed change and sedimentation to reefs along west-central Guam. *Coral Reefs* **33**, 733–749.

PUB (2013) PUB Annual Report 2012/2013. Public Utilities Board, Singapore.

Putten V. E., Dehairs F., Keppens E. and Baeyens W. (2000) High resolution distribution of trace elements in the calcite shell layer of modern *Mytilus edulis*: environmental and biological controls. *Geochim. Cosmochim. Acta* **64**, 997–1011.

R Core Team (2014) A language and environment for statistical computing. R Foundation for Statistical Computing, Vienna.

Rizal S., Damm P., Wahid M. A., Sundermann J., Ilhamsyah Y., Iskandar T. and Muhammad (2012) General circulation in the Malacca Strait and Andaman Sea: a numerical model study. *Am. J. Environ. Sci.* **8**, 479–488.

Robinson R. A., Tong H. and Tham A. K. (1953) A study of drift in the Malacca and Singapore Straits from salinity determinations. In *Proceedings of the 4th Indo-Pacific Fisheries Commission Symposium*, pp. 105–110.

Sebens K. P., Vandersall K. S., Savina L. A. and Graham K. R. (1996) Zooplankton capture by two scleractinian corals, *Madracis mirabilis* and *Montastrea cavernosa*, in a field enclosure. *Mar. Biol.* **127**, 303–317.

Saha N., Webb G. E. and Zhao J.-X. (2016) Coral skeletal geochemistry as a monitor of inshore water quality. *Sci. Total Environ.* **566–567**, 652–684.

Shen C.-C., Lee T., Chen C.-Y., Wang C.-H., Dai C.-F. and Li L.-A. (1996) The calibration of D[Sr/Ca] versus sea surface temperature relationship for *Porites* corals. *Geochimica et Cosmochima Acta* **60**, 3849–3858.

Shen G. T. and Boyle E. A. (1988) Determination of lead, cadmium and other trace metals in annually-banded corals. *Chem. Geol.* **67**, 47–62.

Shue C. L. (2017) Evaluating Impact of passing ship-vessel on coastal hydrodynamics using XBeach. MSc thesis for the. National University of Singapore, Singapore.

Sin T. M., Ang H. P., Buurman J., Lee A. C., Leong Y. L., Ooi S. K., Steinberg P. and Teo S. (2016) The urban marine environment of Singapore. *Reg. Stud. Mar. Sci.* **8**, 331–339.

Sinclair D. J. and McCulloch M. T. (2004) Coral record low mobile barium concentrations in the Burdekin River during the 1974 flood: evidence for limited Ba supply to rivers? *Palaeogeogr. Palaeoclimatol. Palaeoecol.* **214**, 155–174.

Sinclair D. J. (2005) Non-river flood barium signals in the skeletons of corals from coastal Queensland, Australia. *Earth Planet. Sci. Lett.* **237**, 354–369.

Singstat, 2016. Population trends. Department of Statistics, Ministry of Trade & Industry, Republic of Singapore.

Stecher H. A. and Kogut M. B. (1999) Rapid barium removal in the Delaware estuary. *Geochim. Cosmochim. Acta* **63**, 1003–1012.

Stecher H. A., Krantz D. E., Lord C. J., Luther G. W. and Bock K. W. (1996) Profiles of strontium and barium in *Mercenaria mercenaria* and *Spisula solidissima* shells. *Geochim. Cosmochim. Acta* **60**, 3445–3456.

Stock J. D. and Tribble G. W. (2010) Erosion and sediment loads from two Hawaiian watersheds. *2nd Joint Federal Interagency Conference, Las Vegas*.

Susic M., Boto K. and Isdale P. J. (1991) Fluorescent humic acid bands in coral skeletons originate from terrestrial runoff. *Mar. Chem.* **33**, 91–104.

Tanggang F. T., Xia C., Qiao F., Juneng L. and Shan G. (2011) Seasonal circulations in the Malay Peninsula Eastern continental shelf from a wave-tide-circulation coupled model. *Ocean Dynamics* **61**, 1317–1328.

Tanzil J. T. I., Lee J. N., Brown B. E., Quax R., Kaandorp J. A., Lough J. M. and Todd P. A. (2016) Luminescence and density banding patterns in massive *Porites* corals around the Thai-Malay Peninsula, Southeast Asia. *Limnol. Oceanogr.* **61**, 2003–2026.

The Iolite Team (2017) Iolite 3 User's Manual. School of Earth Science, University of Melbourne, Australia.

Tudhope A. W., Lea D. W., Shimmield G. B., Chilchott C. P. and Head S. (1996) Monsoon climate and Arabian Sea coastal upwelling recorded in massive corals from Southern Oman. *PALAIOS* **11**, 347–361.

Tun, K., 2012. Optimisation of reef survey methods and application of reef metrics and biocriteria for the monitoring of sediment-impacted reefs. PhD Thesis for the National University of Singapore, Singapore.

Tun K., Cheshire A. C. and Chou L. M. (1994) Photosynthetic production of four scleractinian corals from Singapore. 3rd ASEAN-Australia Symposium on Living Coastal Resources 2, 69–77.

Walther B. D., Kingsford M. J. and McCulloch M. T. (2013) Environmental records from Great Barrier Reef corals: inshore versus offshore drivers. *PLoS One* **8**, e77091.

Wood S. N. (2006) Generalized additive models: an introduction with R. In *Texts in Statistical* (eds. B. P. Carlin, C. Chatfield, M. Tanner and J. Zidek). Chapman and Hall/CRC Press, Florida, pp. 59–325.

Zicheng P., Xuexian H., Zhaofeng Z., Jie Z., Liusi S. and Hui G. (2002) Correlation of coral fluorescence with nearshore rainfall and runoff in Hainan Island, South China Sea. *Progr. Nat. Sci.* **12**, 41–44.

Associate editor: Yuri Amelin